이학박사학위논문

분열성 효모 *Schizosaccharomyces pombe* 내 Aconitase 2에 의한 유전자 발현 조절 연구

Gene regulation by nuclear enzyme Aconitase 2 in *Schizosaccharomyces pombe*

2021 년 2 월

서울대학교 대학원

생명과학부

조수연

Gene regulation by nuclear enzyme Aconitase 2 in *Schizosaccharomyces pombe*

by

Soo-Yeon Cho

under the supervision of

Professor Won-Ki Huh, Ph.D.

A Thesis Submitted in Partial Fulfillment of

the Requirements for the Degree of

Doctor of Philosophy

February, 2021

School of Biological Sciences

Graduate School

Seoul National University

분열성 효모 *Schizosaccharomyces pombe* 내 Aconitase 2에 의한 유전자 발현 조절 연구

지도교수 허 원 기

이 논문을 이학박사 학위논문으로 제출함

2020년 12월

서울대학교 대학원

생명과학부

조 수 연

조수연의 이학박사 학위논문을 인준함

2020년 12월

위 원 장 성 영 철 (인)

부 위 원 장 허 원 기 (인)

위 원 노 정 혜 (인)

위 원 강 현 아 (인)

위 원 김 경 동 (인)

ABSTRACT

Organisms have devised an efficient way of regulating gene expression while sensing environmental stress. A unique example is a regulatory mechanism through a moonlighting metabolic enzyme such as mammalian aconitase. Aconitase, well-known as a mitochondrial TCA cycle enzyme, senses iron deficiency and acts as an iron regulatory protein (IRP) in mammals and metazoa, controlling the expression of mRNA related to iron homeostasis. From prokaryotes to mammals, multiple functions of aconitase have been reported. A recent study from our lab revealed that aconitase 2 (Aco2) in *Schizosaccharomyces pombe*, a fusion protein of aconitase and a mitochondrial ribosomal protein, exists in the nucleus in addition to mitochondria, and that it is required for protein translation in mitochondria and controls heterochromatin formation in the nucleus. More study is in need to unravel the role of Aco2 in the nucleus.

Considering the conserved function of aconitase in various organisms, Aco2 is likely to interact with nucleic acids or proteins to regulate gene expression. To investigate the role of nuclear Aco2, phenotypes of *aco2* mutant devoid of nuclear localization signal (NLS) (*aco2ΔNLS)* were examined. Transcriptome analysis revealed that the mutation caused increase in mRNAs coding for iron uptake transporters, such as Str1, Str3, Shu1. mRNA decay assay and RT-qPCR analysis showed that the half-life of iron uptake mRNAs increased in *aco2ΔNLS*, suggesting that the nuclear Aco2 may function in the degradation of those mRNAs. UV crosslinking RNA-IP (CLIP) analysis revealed that Aco2 directly binds to iron transporter mRNAs. Among exoribonuclease candidates, Rrp6 and Caf1 appear to affect degradation of these mRNAs. Co-IP experiments of Aco2-FLAG with Rrp6-TAP demonstrated that they interact physically. Therefore, it is concluded that nuclear Aco2 facilitates iron uptake mRNAs to be degraded by exoribonucleases such as Rrp6 under iron-sufficient conditions. Aco2 contributes to maintain intracellular iron homeostasis through post-transcriptional regulation of iron transporter genes.

From transcriptome analysis and respiration-defective phenotype of *aco2ΔNLS* mutant, it is hypothesized that nuclear Aco2 may regulate genes involved in cellular respiration. Most of gene expressions for nuclear-encoded electron transport chain (ETC) were decreased by about 2-fold in *aco2ΔNLS*. mRNA decay assay revealed that the decay rate of ETC mRNAs in

aco2ΔNLS did not changed, indicating Aco2 may be involved in transcriptional regulation of ETC genes. Therefore, whether Aco2 interacts with the transcription factors of ETC genes or Aco2 itself regulates the expression of ETC genes as a transcription factor are needed to be demonstrated.

This study newly discovered that *S. pombe* Aco2 regulates genes related to iron homeostasis and cellular respiration. Specially, a new mechanism for maintaining iron homeostasis was revealed that Aco2 regulates the expression of iron-uptake genes at the post-transcriptional level. Given the unique features of the moonlighting enzyme and dual targeting, Aco2 is expected to play another important role in maintaining the life of cells.

Keywords: Fission yeast, Aconitase, Iron-regulatory protein, moonlighting enzyme, mRNA degradation, post-transcriptional regulation, electron transport chain (ETC), cellular respiration

CONTENTS

LIST OF FIGURES

LIST OF TABLES

ABBREVIATIONS

a.a.	amino acid
AD	aconitase domain
cDNA	complementary DNA
co-IP	co-immunoprecipitation
Ct	cycle threshold
DAPI	4′,6-diamidino-2-phenylindole
DEGs	differentially expressed genes
DNA	deoxyribocunleic acid
dsRNA	double-stranded RNA
dT	deoxythymidine
DTT	dithiothreitol
ECL	enhanced chemiluminescence
EDTA	ethylene-diamine-tetraacetic acid
EMM	Edinburgh minimal medium
ETC	electron transport chain
FC	fold change
GFP	green fluorescence protein
GO	gene ontology
IP	immunoprecipitation
IRE	iron-responsive element
IRP	iron regulatory protein
Kb	kilo base pair
kDa	kilo dalton
LS-MS	liquid chromatography–mass spectrometry
Mb	mega base pair
mRNA	messenger RNA

MTS	mitochondrial targeting sequence
NCBI	National Center for Biotechnology Information
NLS	nuclear localization signal
O.D.	optical density
PAGE	polyacrylamide gel electrophoresis
PCR	polymerase chain reaction
PMSF	phenylmethylsulfonyl fluoride
qPCR	quantitative PCR
RD	ribosomal domain
RISC	RNA-induced silencing complex
RNA	ribonucleic acid
RNAi	RNA interference
RT	reverse transcription
S.E.M.	standard error of the mean
SDS	sodium dodecyl sulfate
seq	sequencing
siRNA	small interfering RNA
ssDNA	single-stranded DNA
TCA	tricarboxylic acid
TDW	triple distilled water
UTR	untranslated region
UV	ultraviolet
WT	wild-type

CHAPTER I. INTRODUCTION

I-1. Fission yeast *S. pombe* as a model organism

Schizosaccharomyces pombe is a rod-shaped, unicellular eukaryote which is ~7–14 μm in length and ~4 μm wide. *S. pombe* has a typical eukaryotic cell cycle with a generation time in vegetative growth of 2~3 h at 30~32℃ in rich media and minimal media (Fig. I-1).

S. pombe was originally found in contaminated millet beer due to a delay in journey from East Africa to Germany. In 1893, Paul Lindner named it "*Schizo*"-*saccharomyces* because it divided by binary fission, unlike budding yeast *Saccharomyces*. The species name *pombe* means beer in Swahili (Hayles and Nurse, 2018). It has been widely known since Paul Nurses, Lee Hartwell and Tim Hunt used it as a model system to study cell cycle regulation and received the 2001 Nobel Prize in Physiology or Medicine.

The sequence of *S. pombe* genome was fully sequenced in 2002, making it the fourth eukaryote to be fully sequenced. It has a ~14 Mb genome; 5.6, 4.8, and 3.6 Mb, respectively, for Chromosomes I, II, and III. The size of mitochondrial DNA is 19.4 kb. Currently 5059 protein-coding genes are annotated and ~ 70% of them are conserved in human (Wood et al., 2002) (Fig. I-1). In addition to cell cycle, genome organization or chromosome structure of *S. pombe* are very similar to higher eukaryotes, so that it is a very useful to study heterochromatin (Cam and Whitehall, 2016).

A

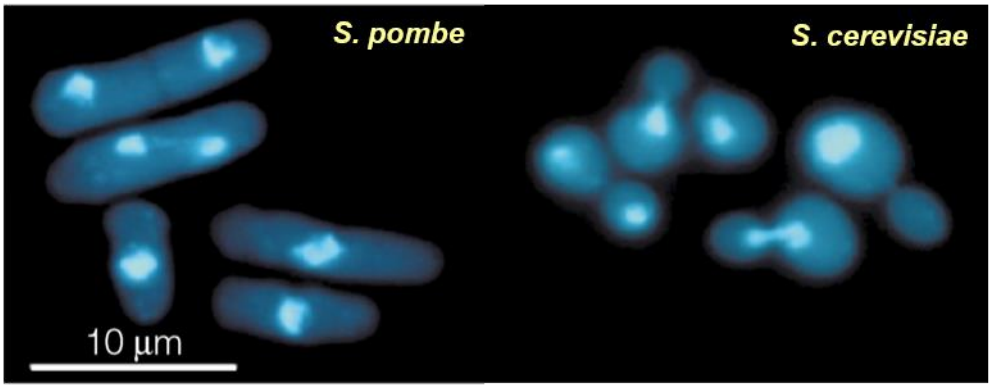

B

Cell shape	Rod-shaped, unicellular	
Cell size	7~14 um in length, ~4 um in diameter	
Generation time	2~3 h (in complex or minimal media)	
Optimal temperature	30~32°C	
Genome size	~14 Mb	Chr I: 5.6 Mb Chr II: 4.8 Mb Chr III: 3.6 Mb mtDNA: 19.4 kb
# of Protein-coding genes	5059	

Figure I-1. Introduction of fission yeast as a model organism

(A) Cell morphology of fission yeast *S. pombe* and budding yeast *S. cerevisiae*. Cells were stained with DAPI (Forsburg, 2001). (B) Basic information of *S. pombe* (Hayles and Nurse, 2018)

I-2. A moonlighting enzyme, aconitase

During evolution, organisms has adapted an efficient way to detect environmental stress and at the same time regulate gene expression. Mechanisms of gene regulation through cytoplasmic or mitochondrial metabolic enzymes have been revealed. Most of enzymes involved in glycolysis are observed in the nucleus and known to control histone modification or transcription. Nuclear functions of some mitochondrial TCA cycle enzymes have been reported: IDH2 (Isocitrate dehydrogenase 2) is involved in histone and DNA methylation and Fumarase is involved in DNA repair (Boukouris et al., 2016) (Fig. I-2).

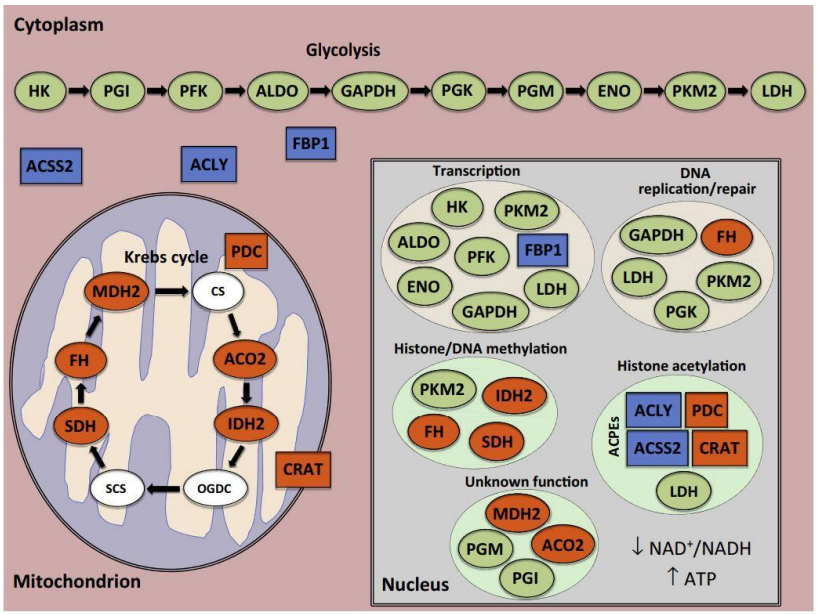

Figure I-2. Moonlighting metabolic enzymes

Cytoplasmic (glycolytic (green) and non-glycolytic (blue)) and mitochondrial enzymes are known to translocate into the nucleus. While all the essential glycolytic enzymes are found in the nucleus, only some Krebs cycle (TCA cycle) enzymes have been described in the nucleus (orange) whereas others have not (white). According to their nuclear function, the enzymes are grouped together (Boukouris et al., 2016).

*Abbreviations: ACLY, ATP citrate lyase; ACO2, aconitase 2; ACPEs, acetyl-CoA-producing enzymes; ACSS2, acetyl-CoA synthetase short-chain family member 2; ALDO, fructose bisphosphate aldolase; CRAT, carnitine acetyltransferase; CS, citrate synthase; ENO, enolase; FBP1, fructose-1,6-bisphosphatase; FH, fumarate hydratase; GAPDH, glyceraldehyde 3-phosphate dehydrogenase; HK, hexokinase; IDH2, isocitrate dehydrogenase 2; LDH, lactate dehydrogenase; MDH2, malate dehydrogenase 2; OGDC, /-ketoglutarate dehydrogenase; PDC, pyruvate dehydrogenase complex; PFK, phosphofructokinase; PGI, phosphoglycerate isomerase; PGK, phosphoglycerate kinase; PGM, phosphoglycerate mutase; PKM2, pyruvate kinase M2; SCS, succinyl-CoA synthetase; SDH, succinate dehydrogenase

Mammalian cytosolic aconitase is the representative example of “moonlighting” metabolic enzyme. Aconitase is originally known as a TCA cycle enzyme that converts citrate to isocitrate. It can also regulate the expression of genes involved in iron homeostasis depending on the concentration of iron in cells, at this time called IRP (iron regulatory protein). In iron-deficient cells, cytosolic aconitase (c-aconitase) loses iron-sulfur cluster and is switched to IRP through conformational change. IRP gains the ability to bind RNAs so called iron-responsive elements (IREs) (Fig. I-3). IRE is an RNA-stem loop structure, located in untranslated region (UTR) of mRNAs encoding functions in iron homeostasis. Under iron-deficient condition, IRP inhibits the translation by binding to IREs in 5’ UTR of iron-consuming mRNAs and stabilizes iron uptake mRNAs by binding to IREs in 3’ UTR. Under iron-sufficient condition, IRP acts as the aconitase, having an iron-sulfur cluster which is required for catalytic activity (Tandara and Salamunic, 2012) (Fig. I-4).

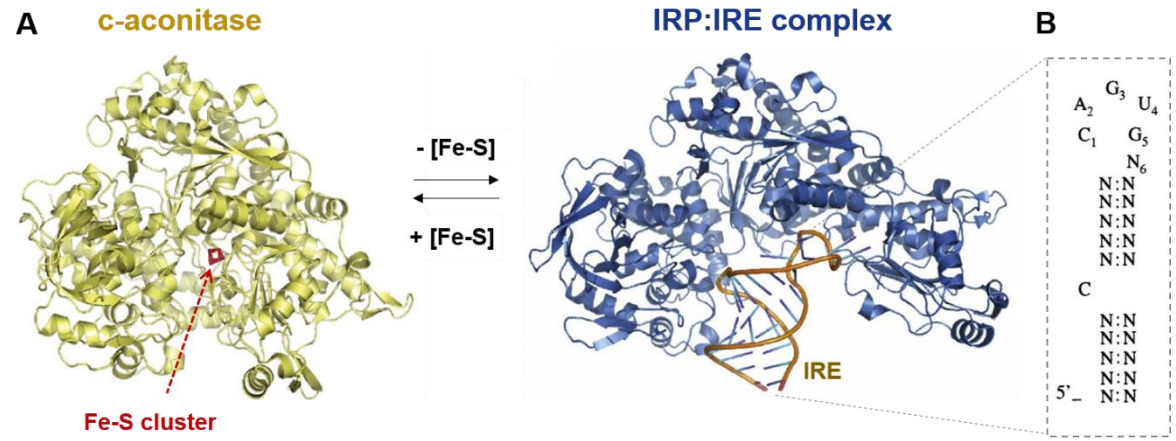

Figure I-3. c-Aconitase functions as Iron regulatory protein (IPR)

(A) Conformational change of IRP. Under iron-deficient condition, c-aconitase loses Fe-S cluster and acts as IRP. IRP binds to specific RNA structure called iron responsive element (IRE) located in UTR of iron homeostasis mRNAs (Castello et al., 2015). (B) Conserved sequence and secondary structure of IRE (Alen and Sonenshein, 1999).

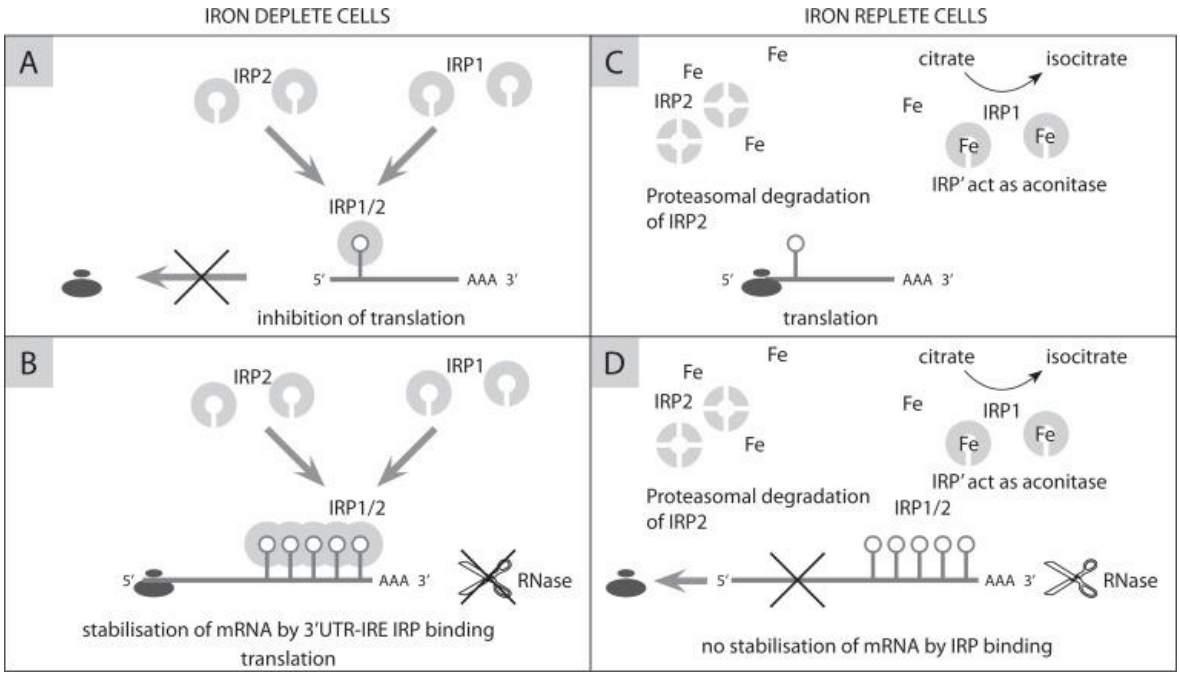

Figure I-4. Maintenance of cellular iron homeostasis by IRE/IRP system

(A) In iron-deplete cells, binding of IRP at 5′ UTR IRE of iron efflux or iron storage mRNAs block translation inhibiting its initiation. (B) Binding of IRP at 3′ UTR IRE of iron uptake mRNA stabilize its transcript. (C) In iron-replete cells, IRP act as aconitase. (D) In presence of sufficient iron, there is no binding of IRP and stabilization of iron uptake mRNA (Tandara and Salamunic, 2012).

In addition to mammalian IRP, multiple functions of aconitase have been reported from bacteria to other higher eukaryotes. In *E. coli* and *B. subtilis*, aconitase (AcnB) functions as IRP, binding to iron uptake mRNAs or *acnB* own mRNA (Benjamin and Masse, 2014). In *C. crescentus*, aconitase is the major component of the RNA degradosome (Hardwick et al., 2011) (Fig. I-5). In *S. cerevisiae*, Aco1 binds to mitochondrial DNA and protect it from accumulation of point mutation and ssDNA break (Chen et al., 2007). In *C. elegans*, a genome-wide screening has revealed that *aco-2* gene, along with known genes involved in RNA interference (RNAi) machinery and heterochromatin formation, is the required genetic component for RNAi (Kim et al., 2005). But still lack of studies on new function of aconitase in *S. pombe*.

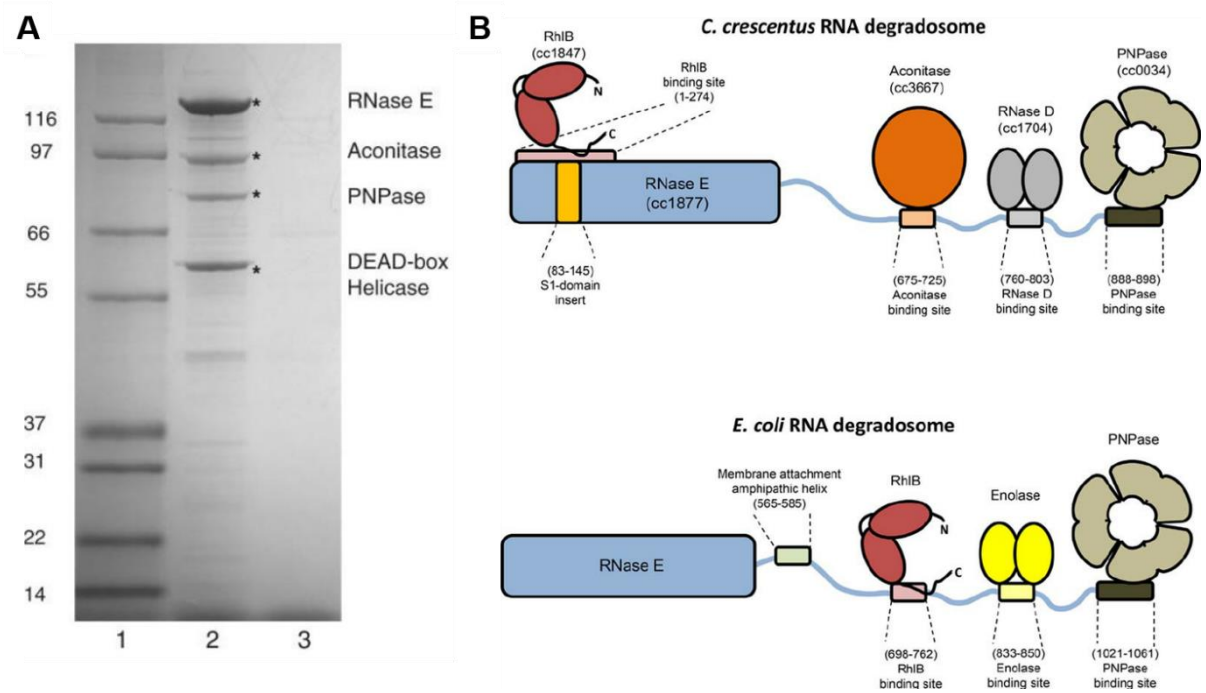

Figure I-5. Aconitase as the RNA degradosome component in *C. crescentus*

(A) SDS-PAGE analysis of cell lysates immunoprecipitated using RNase E antibody (Hardwick et al., 2011) (B) A schematic model of *C. crescentus* RNA degradosome in comparison to that of *E. coli* (Voss et al., 2014)

*RhlB, DEAD-box RNA helicase; RNase E, endoribonuclease; RNase D, exoribonuclease; PNPase, exoribonuclease polynucleotide phosphorylase; Enolase, glycolytic enzyme

I-3. Two types of aconitases in *S. pombe*

There are two genes encoding aconitase in *S. pombe*: *aco1*, *aco2*. Aco1 and Aco2 protein show ~80% sequence similarity according to NCBI-protein alignment analysis. Both have conserved cysteine residues binding with Fe-S cluster, required for their catalytic activity. Both genes are essential for cell viability (Kim et al., 2010) (Hayles et al., 2013). In a single cell, grown in minimal media, about 40,000 to 100,000 molecules of Aco1 and about 22,500 to 50,000 molecules of Aco2 exist during mitosis or vegetative growth phase (Carpy et al., 2014). Most of them locate in mitochondria (Matsuyama et al., 2006).

.

I-4. Distinctive features of *S. pombe* Aconitase 2

Unlike Aco1, Aco2 is observed in not only mitochondria but also nucleus and cytosol. This is because Aco2 is a fusion protein consisting of an aconitase and a mitochondrial ribosomal protein L21, containing both mitochondrial targeting sequence (MTS) in the aconitase domain and nuclear localization signal (NLS) in the ribosomal domain (Fig. I-6). Our research group first reported the dual targeting of Aco2 in 2015. Although the exact ratio of nuclear Aco2 and mitochondrial Aco2 is not yet found out, it is mostly observed in mitochondria. The uneven distribution of Aco2 in the cell occurs because the RNA of Aco2 is transcribed into two types through alternative termination: a short transcript that is transcribed only to the aconitase domain, and a long transcript that is transcribed to the ribosomal domain (Fig. I-7B, 7C). Accordingly, Aco2 protein is also translated into two sizes: about 100 kDa and 89 kDa, respectively (Fig. I-7A). Aco2 with only MTS is more produced so that it is abundant in mitochondria. The questions still remain to what is the mechanism of dual targeting of Aco2 or environmental signals of inducing the nuclear Aco2.

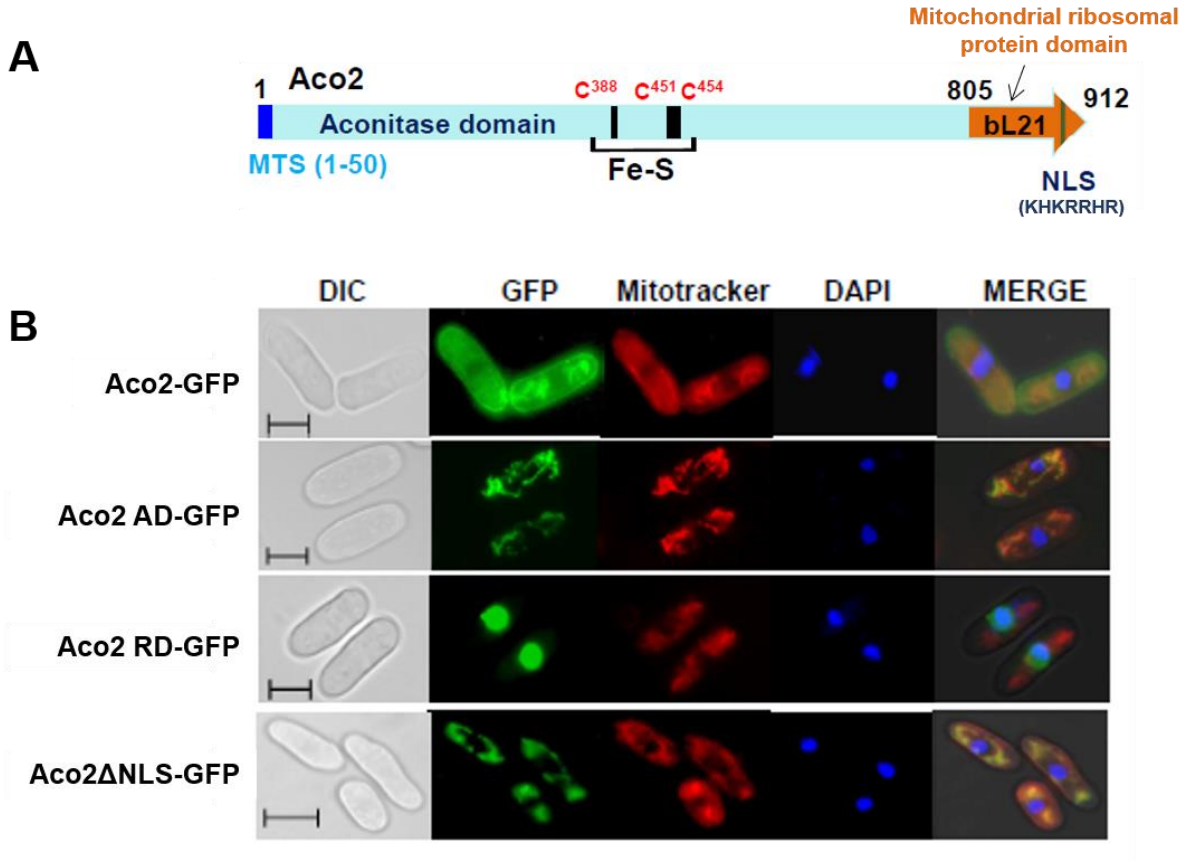

Figure I-6. Dual targeting of *S. pombe* Aco2

(A) A schematic diagram of Aco2 in *S. pombe*. Aco2 contains MTS (MKLCLSGSSQAIPSK-GISLVAARFQSTASRASYVTPPYEKLMGKLQQVRK) at N-terminus of aconitase domain and NLS (KHKRRHR) at C-terminus of bL21 ribosomal domain. Its conserved cysteine residues (C388, C451, C454) were also shown. (B) Intracellular localization of Aco2-GFP. Wild-type Aco2 observed in mitochondria, nucleus and cytosol. When NLS of Aco2 is deleted, location of Aco2 is limited to mitochondria. (Jung et al., 2015)

*MTS, mitochondrial targeting sequence; NLS, nuclear localization signal; AD, aconitase domain; RD, mitochondrial ribosomal domain

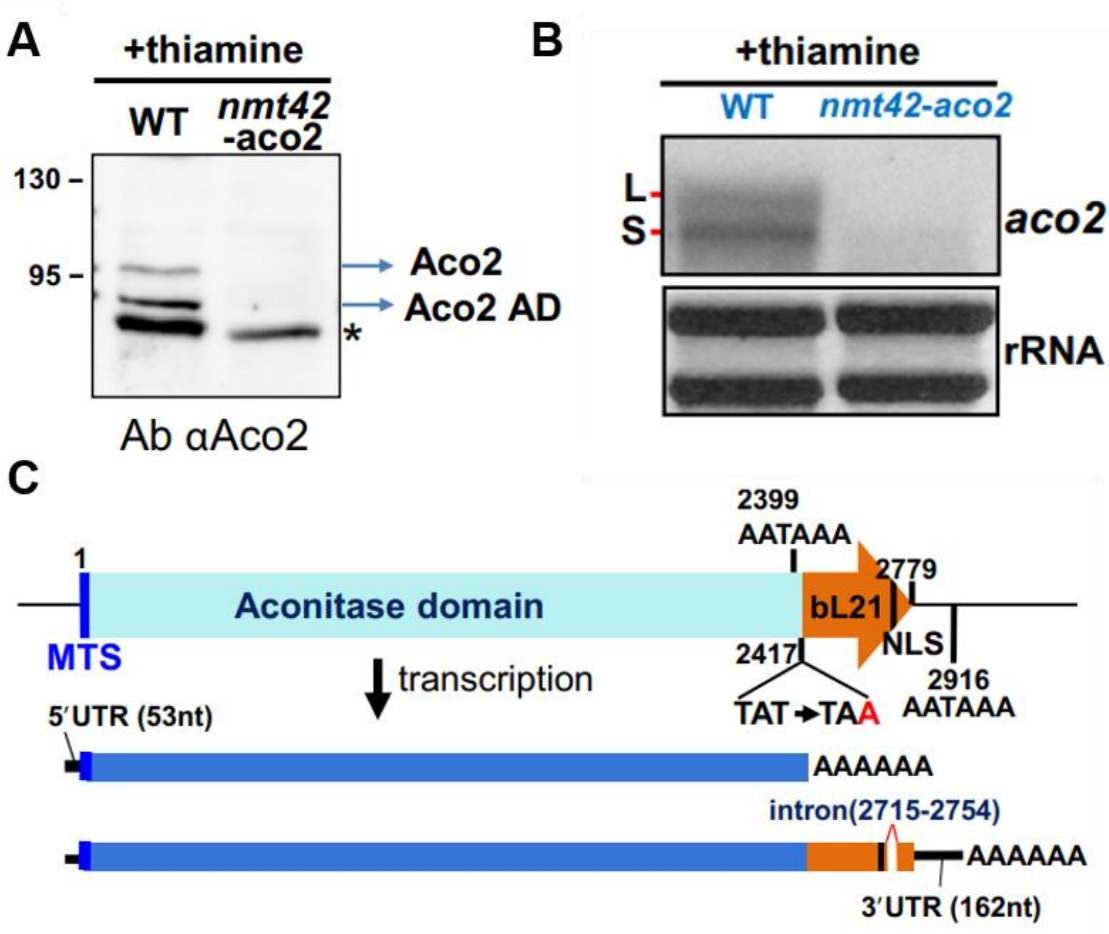

Figure I-7. Two types of Aco2 generated though alternative termination

(A) Western blot analysis using anti-aconitase antibody. The estimated size of each Aco2 protein is as follow: Aco2 (918 a.a.), ~100 kDa; Aco2 AD (805 a.a.), ~89 kDa (B) Northern blot analysis of *aco2* transcript in wild-type. (C) a diagram of two *aco2* transcripts produced by alternative termination. (Jung et al., 2015)

*AD, aconitase domain; Ab αAco2, anti-aconitase antibody; L, a long transcript; S, a short transcript

I-5. Novel functions of Aco2 depending on its intracellular location

A senior researcher in our research team presented the novel functions of *S. pombe* Aco2. A pulse-chase ^{35}S-methionine labeling assay revealed that mitochondrial Aco2 is responsible for mitochondrial translation and its ribosomal domain is required for that role. The loss of cell viability by *aco2* deletion was restored not by the aconitase domain but by the bL21 ribosomal domain. The reason why Aco2 protein is essential in cells is probably because it contributes to mitochondrial protein synthesis (Jung et al., 2015) (Fig I-8).

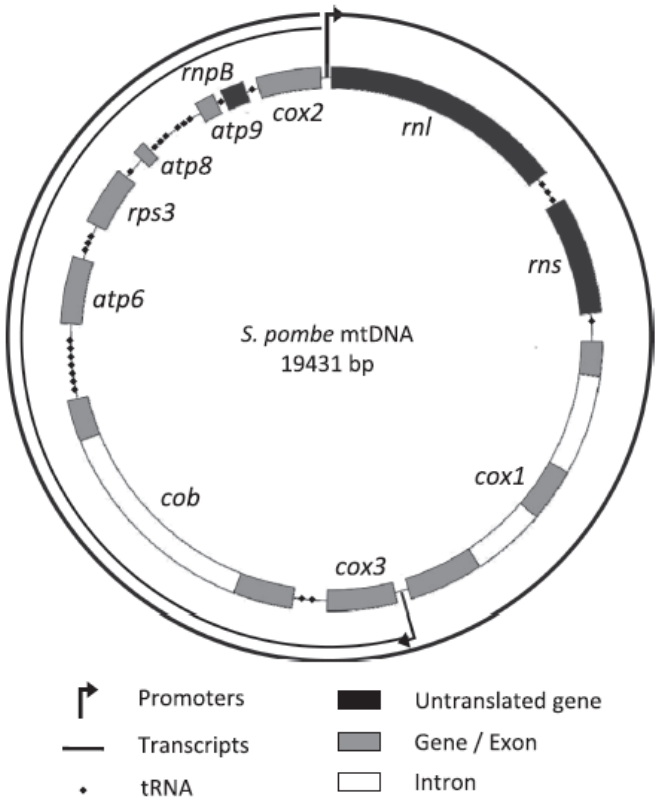

Figure I-8. Mitochondrial DNA (mtDNA) in *S. pombe*

A Map of *the S. pombe* mtDNA (Kuhl et al., 2011). It encodes key subunits of the oxidative phosphorylation (OXPHOS) complexes, such as cytochrome b of cytochrome b-c1 complex (complex III) (Cob), cytochrome c oxidase (complex IV) subunits 1, 2, 3 (Cox1, 2, 3) and ATP synthase (complex V) subunits (Atp6, 8, 9). (Liu et al., 2018)

Since aconitase has been reported to be involved in the RNAi pathway in *C. elegans* (Kim et al., 2005), the effect of nuclear Aco2 in heterochromatin formation was examined. Genetic and physical interaction of Aco2 with heterochromatin assembly factors like Chp1 (Fig. I-9) and its effect on modulating transcription from the centromeric and subtelomeric regions were investigated. As a result, Aco2 was found out to function as an anti-silencing factor in the heterochromatin region (Jung et al., 2019).

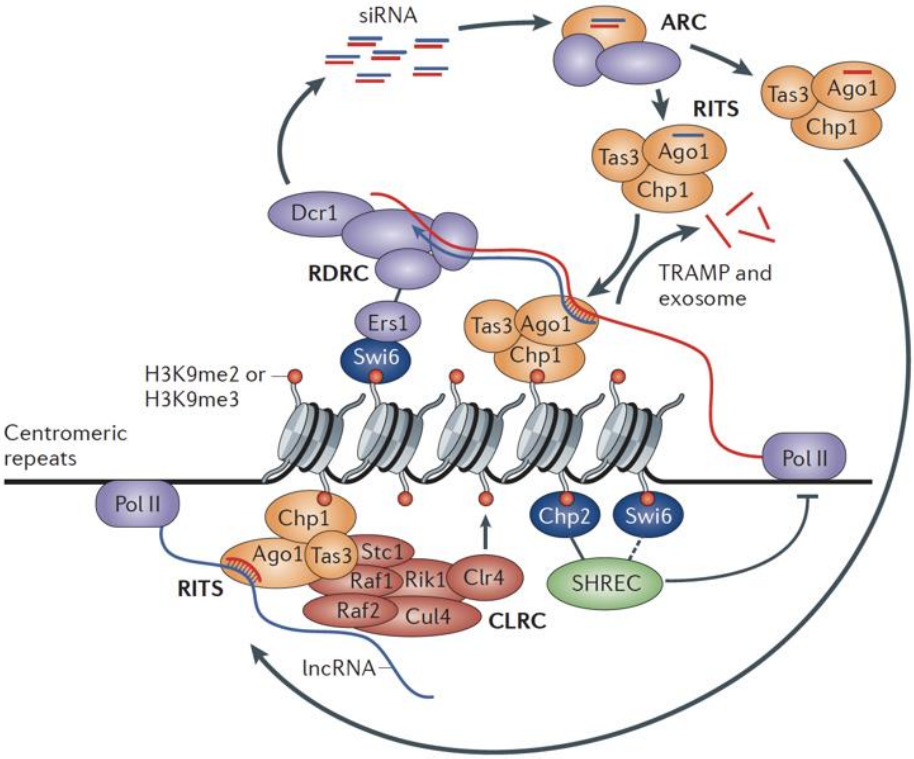

Figure I-9. RNAi-mediated heterochromatin assembly in *S. pombe*

The RNA-induced transcriptional silencing (RITS) complex composed of Ago1, Chp1, and Tas3 interacts with the nascent RNA transcripts via siRNA-RNA base pairing. The RITS complex binds to H3K9me (histone H3 methylated at lysine 9) via Chp1 and then recruits CLRC (Clr4-Rik1-Cul4 methyltransferase complex). CLRC initiates H3K9 methylation. The RITS complex also recruits RDRC (RNA-dependent RNA polymerase complex)/Dicer and promotes dsRNA synthesis and siRNA production. siRNAs are delivered to the RITS complex through the ARC (Argonaute siRNA chaperone). (Holoch and Moazed, 2015)

I-6. Maintenance iron homeostasis in *S. pombe*

Iron is an essential cofactor for a wide variety of proteins involved in respiration and tricarboxylic acid cycle, DNA replication and repair (Touati, 2000). On the other hand, excess iron is toxic to cells because of its redox-active property, which can generate reactive oxygen species (ROS) via Fenton reaction. Therefore, intracellular iron homeostasis must be highly regulated to prevent both iron starvation and toxicity (Pelletier et al., 2005).

In general, cellular iron homeostasis is controlled by a post-transcriptional regulatory mechanism involving iron regulatory proteins (IRP) and iron responsive elements (IRE) in target mRNAs. However, the regulation of iron homeostasis by IRP in the fission yeast has not been reported.

Under high-iron conditions, Fep1 specifically interacts with GATA elements within the genes involved in reductive iron import (*fio1, frp1*), siderophore transport (*str1, str2, str3*) (Pelletier et al., 2002; Pelletier et al., 2003) and vacuolar transport (*abc3*) (Pouliot et al., 2010). The repressor function of Fep1 requires the presence of the Tup11 or Tup12 transcriptional co-repressor. The iron-sensing depends on the Grx4 which coordinates Fe-S cluster. Together with a BolA-type protein Fra2, Grx4 binds to the C-terminus Fep1, the N-terminus of Fep1 is available for DNA binding (Kim et al., 2011) (Jacques et al., 2014). Grx4 can also bind to the repressor Php4 and inactivate it. The absence of Php4 enables iron-using genes (*pcl1, sdh4, isa1*) to be expressed through the CCAAT-binding Php2/3/5 complex.

Under low-iron conditions, Grx4 loses Fe-S cluster and associates with the N-terminus of Fep1, preventing its repressive effect on iron-uptake gene expression. In contrast, Grx4 dissociates from Php4, resulting in Php4 binds to the Php2/Php3/Php5 complex and then represses the transcription of iron-using genes. When iron is scarce, Fe^{3+} is reduced to Fe^{2+} by the Frp1 cell surface reductase. Fe^{2+} is oxidized to Fe^{3+} by the Fio1 ferroxidase and then transported across the plasma membrane by the Fip1 permease. Siderophore-iron transporters Str1, Str2 and Str3 are active as well as Abc3 which transports stored iron from the vacuole to the cytoplasm (Labbe et al., 2013) (Fig I-10).

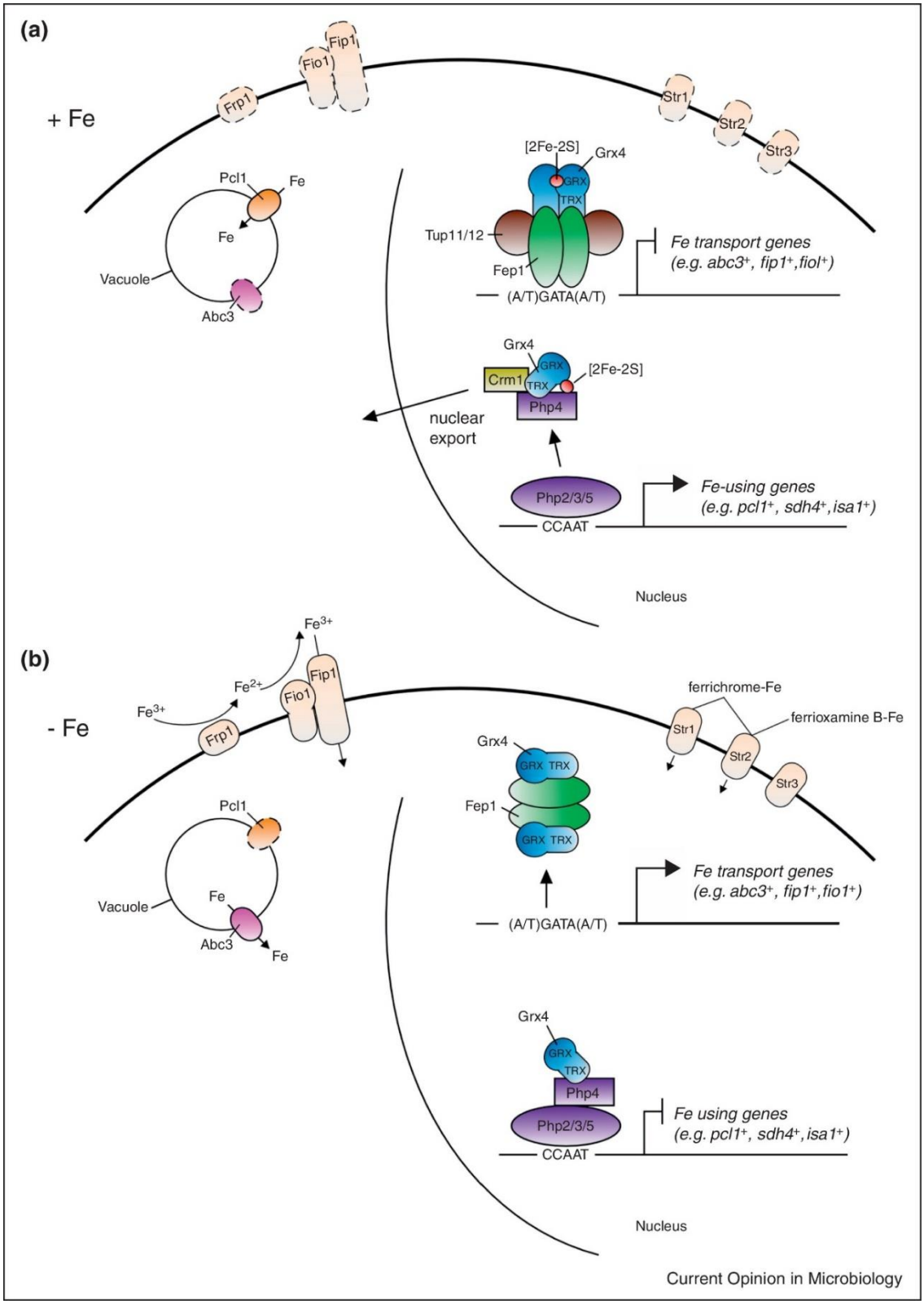

Figure I-10. Iron uptake and regulation in *S. pombe*

(Labbe et al., 2013)

I-7. Post-transcriptional gene regulation in eukaryotes

There are two general pathways of mRNA decay have been identified in eukaryotic cells. mRNA degradation usually begins with the shortening of the poly(A) tail at the 3′ end of the mRNA (deadenylation) by a variety of mRNA deadenylases. Following deadenylation, a decapping enzyme consisting of two subunits, Dcp1p and Dcp2p, removes the 5′ cap structure, exposing the transcript to digestion by a 5′→3′ exonuclease, Xrn1p. Alternatively, after deadenylation, mRNAs can be degraded in a 3′→5′ direction by the cytoplasmic exosome, a complex of diverse 3′→5′ exonucleases. The degradation of individual mRNAs can also be initiated by endonuclease cleavage either by sequence-specific endonucleases, or in response to miRNAs or siRNAs (Parker and Song, 2004) (Fig I-11).

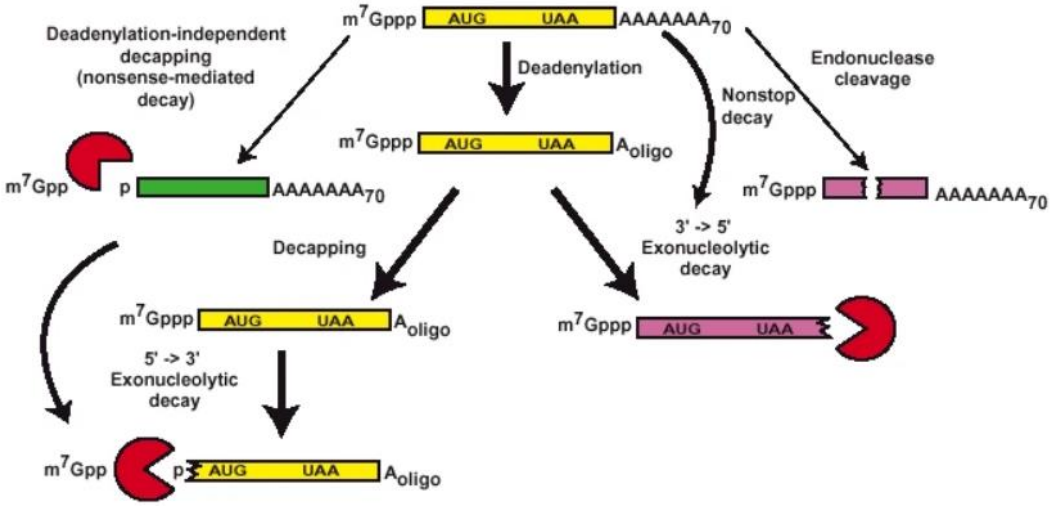

5'-3' exoribonuclease activity (GO:0004534)	
Exo2	exonuclease II
Dhp1	5'-3' exoribonuclease Dhp1
3'-5'-exoribonuclease activity (GO:0000175)	
Caf1	CCR4-Not complex CAF1 family ribonuclease subunit
Ccr4	CCR4-Not complex 3'-5'-exoribonuclease subunit
Dis3	exosome 3'-5' exoribonuclease subunit
Rrp6	exosome 3'-5' exoribonuclease subunit
Nuclear-transcribed mRNA catabolic process, exonucleolytic, 3'-5' (GO:0034427)	
Dis32	3'-5'-exoribonuclease activity Dis3L2

Figure I-11. Pathways of eukaryotic mRNA turnover

Enzymes and control of eukaryotic mRNA turnover are shown (Parker and Song, 2004). Exoribonucleases involved in mRNA catabolic process in *S. pombe* are shown below.

CHAPTER II. MATERIALS AND METHODS

II-1. Strains and Culture conditions

Fission yeast strains used in this study are listed in Table II-1. Standard cell culture methods and media as previously described (Forsburg and Rhind, 2006) were used: YE rich media (0.5% yeast extract and 3% glucose), EMM minimal media (0.3% potassium hydrogen phthalate, 0.56% $Na_2HPO_4 \cdot 12H_2O$, 0.5% NH_4Cl, 2% glucose, 20 ml/L salts stock (50x), 1 ml/L vitamins stock (1,000x), and 0.1 ml/L minerals stock (10,000x)). For auxotrophic strains, supplements (leucine, adenine, and uracil, 250 mg/L each) were added to culture media as appropriate. Cells were grown at 30°C or 32°C.

II-2. Yeast transformation

For fission yeast competent cells, cells were harvested at $O.D._{600}$ =0.5~0.8. Cells were pelleted by centrifugation at 4°C, 4000 rpm. Collected cells were kept on ice, and washed with distilled water and 1.2 M sorbitol. After resuspended in ~100 ul of 1.2 M sorbitol, cells were mixed with recombinant DNA (circular or linear form) and moved to cuvette (MicroPulser electroporation cuvette, Bio-Rad) for electroporation. Electroporation was performed with the operation option for *S. pombe* (MicroPulser electroporator, Bio-Rad). Cells were regenerated for 2~4 h or overnight in 4 ml of EMM media or 1/2 diluted YE media at 30°C. Regenerated cells were spread on solid media (with the addition of antibiotics, if necessary).

II-3. Genomic DNA extraction

To extract the chromosomal DNA of fission yeast, the extraction buffer was prepared as 0.5 M NaCl, 0.2 M Tris-Cl (pH 7.6), 0.01 M EDTA, 1% SDS. Harvested cells were lysed with 400 ul of extraction buffer and 400 ul of phenol, and then centrifuged at 13,200 rpm for 10~15 min. The supernatant was mixed with equal volume of chloroform and centrifuged again. The supernatant was precipitated with 750 ul of 100% ethanol. DNA pellet was washed with 70% ethanol, and dissolved in TDW.

Table II-1. Fission yeast strains used in this study

Name	Description	Source
WT(665)	*h- ade6-M210 leu1-32 ura4-D18*	Lab. Stock
aco2ΔNLS	*h- ade6-M210 leu1-32 ura4-D18 aco2ΔNLS::natMX*	Jung et al. 2015
Fep1-5FLAG	*h- fep1-5FLAG::hphMX*	This study
aco2ΔNLS Fep1-5FLAG	*h- aco2ΔNLS::natMX fep1-5FLAG::hphMX*	This study
JH42	*h- ade6-M210 leu1-32 ura4-D18 leu1-32::leu1*	This study
aco2ΔNLS+leu	*h- ade6-M210 leu1-32 ura4-D18 leu1-32::leu1 aco2ΔNLS::NatMX*	Jung et al. 2019
aco2ΔNLS+Aco2	*h- ade6-M210 ura4-D18 aco2ΔNLS::natMX leu1-32::leu1-Aco2*	Jung et al. 2019
aco2ΔNLS +NLS-AD	*h- ade6-M210 ura4-D18 aco2ΔNLS::natMX leu1-32::leu1-NLS-aco2(51-805)*	Jung et al. 2019
aco2ΔNLS+AD	*h- ade6-M210 ura4-D18 aco2ΔNLS::natMX leu1-32::leu1-aco2(51-805)*	Jung et al. 2019
aco2ΔNLS+RD	*h- ade6-M210 ura4-D18 aco2ΔNLS::natMX leu1-32::leu1-aco2(806-912)*	Jung et al. 2019
aco2ΔNLS +aco2(3CS)	*h- ade6-M210 ura4-D18 aco2ΔNLS::natMX leu1-32::leu1-aco2(C388S,C451S,C454S)*	Jung et al. 2019
Aco2-5FLAG	*h- ade6-M210 leu1-32 ura4-D18 aco2-5FLAG::hphMX*	Jung et al. 2019
caf1Δ	*h+ ade6-M210 leu1-32 ura4-D18 caf1Δ::kanMX*	Bioneer
ccr4Δ	*h+ ade6-M216 leu1-32 ura4-D18 ccr4Δ::kanMX*	Bioneer
dis3-54 (FY9143)	*h- leu1 dis3-54*	Yeast Genetic Resource center (YGRC)
dis32Δ	*h+ ade6-M210 leu1-32 ura4-D18 dis32Δ::kanMX*	Bioneer
exo2Δ	*h+ ade6-M210 leu1-32 ura4-D18 exo2Δ::kanMX*	Bioneer
rrp6Δ	*h+ ade6-M210 leu1-32 ura4-D18 rrp6Δ::hphMX*	Jung et al. 2015
aco2ΔNLS rrp6Δ	*h+ ade6-M210 leu1-32 ura4-D18 aco2ΔNLS::natMX rrp6Δ::hphMX*	Jung et al. 2015
fep1Δ	*h- ade6-M210 leu1-32 ura4-D18 fep1Δ::kanMX*	This study
fep1Δ aco2ΔNLS	*h- ade6-M210 leu1-32 ura4-D18 aco2ΔNLS::natMX fep1Δ::kanMX*	This study

II-4. RNA preparation & analysis

II-4.1. RNA extraction

Total RNA was extracted using Hot-phenol method (Herrick et al., 1990). Cells were grown to $O.D._{600}$= 0.5~1 and harvested. Collected cells were resuspended in 360 μl of AE buffer (50 mM NaOAC pH 5.2, 10 mM EDTA), 40 μl of 10% SDS and equal amount of phenol:chloroform 5:1 solution. Samples were kept cool on ice. After vortexed thoroughly, samples were incubated at 65°C, 2 times for 5 min. After centrifugation at 4°C 10~15 min., 300 ul of the upper aqueous phase was transferred to a new tube. 100 ul of RNA-free TDW was added and then vortexed with addition of 400 ul of phenol:chloroform 5:1 solution. The supernatant was obtained as described above. The aqueous phase in a new tube was mixed with chloroform and centrifuged at 4°C. The upper layer was precipitated with 750 ul of 100% ethanol at -20°C. Collected RNA pellet was washed with 70% ethanol. After dry, RNA pellet was dissolved in RNase-free TDW.

II-4.2. cDNA synthesis and qPCR

To prevent the genomic DNA contamination, DNA was removed by TURBO DNase and DNA-free™ kit (AM1906, Thermo Fisher Scientific) according to the manufacturer's instructions. 100 pmole/ul of random hexamer and RevertAid™ reverse transcriptase (Thermo Fisher Scientific) were used for cDNA synthesis as following the manufacturer's instruction. cDNA was diluted with TDW in a 1:25 ratio. TOPreal™ qPCR premix (Enzynomics) was used for the qPCR reaction. RT-qPCR primers used in this study were displayed in Table II-2.

For mRNA decay assay, 100 pmole/ul of oligo dT primer was used. For UV-crosslinking RNA-IP (CLIP) analysis, a mixture of gene-specific primers (10 pmole/ul each) was used for reverse transcription.

Table II-2. Primers used in this study

Name	Forward sequence (5'->3')	Reverse sequence (3'->5')	Used for	Reference
act1	TGAGGAGCACCCTTGCTTGT	TCTTCTCACGGTTGGATTTGG	RT-qPCR	This study
abc3	GTACGGTATGCAAGAGACTT	AATAGCTTGCCATCTACTGG	RT-qPCR	This study
fio1	TTCGTTTCATTGCCGATAAC	ATCTCCGGTGCTTCAATAAA	RT-qPCR	This study
fip1	CGGTTCCTATCCCTTCAAAT	CAGTGTTGTTCCAACCTAGA	RT-qPCR	This study
str1	CTACTTACTGTCGCTGTTCA	CCGATATAGCACTTCCAACA	RT-qPCR	This study
str3	TGCTCCTTATCCATCATGTC	CGATTGTAAGTAACCCGCTA	RT-qPCR	This study
shu1	GAGACGTCTATACAGCATCG	AACCAAGTAAAGACCTACGG	RT-qPCR	This study
sib1	TCAACAATTTGTAGGTCGGT	CAACAATTCCCACGCAATTA	RT-qPCR	This study
fep1	ATCAATGTCAAATGGACCGA	TGAACTTCAGGAGGAAACTG	RT-qPCR	This study
php2	ACTCACACGTCTGAAGGATA	TTAGCAGGAGACATAGATGC	RT-qPCR	This study
php4	ACCAAGGTTTATGCTCAACT	GGTTCCATGGTAGGAAGTTT	RT-qPCR	This study
php3	GCTTTAAATACCCTTGGGTTC	GACCGGCTTTGTTTAGTTTC	RT-qPCR	This study
php5	GAGGTTGCTAGTCCATTTGA	TTACAGCTTGATCGTCATGT	RT-qPCR	This study
Aco2 NLS	TTTACTCTCTTTGGTAACCC	GCTTGTGTTTTACTCGAACA	RT-qPCR	This study
fra1	GAATGTCATATTCGCGATGG	CGGAATTGTTCAAGTTTGGT	RT-qPCR	This study
frp1	CTCGTTCTTCGGCTTTATTG	CAGGGTAGCTGTTAGTCAAA	RT-qPCR	This study
frp2	TTTCTCATATGGCTGCATCA	AGCGATTCCAAATGCTTCTA	RT-qPCR	This study
tup11	AACTTCTCAGAGTTGGTACG	AAACTTAACGCAGCAAACAA	RT-qPCR	This study
tup12	AATATGGGACATCGCTCAAA	TCCACTACCAGAAACCAATG	RT-qPCR	This study
grx4	CTCTAAAGCTCCAAATGGGT	ATGCAGGTTCTGAAGGAGTA	RT-qPCR	This study
qcr2	GTACTTGTCTGCTTTTGAACCTG	GGCTAATAAAGATGAAACACC	RT-qPCR	This study
qcr9	CTCAGTTTTCGCATTCCATTACC	GCGTAGATTGAAGAGTTTCTTCGG	RT-qPCR	This study
cox13	GAATCGTAACATTGGCTTCCTATC	CCTTTGCTTCGTTACTATAAGCTC	RT-qPCR	This study
cox7	CTATTGTTCAACAACAACGCTTTC	GCATCTTTCTTCCCGAAAATGACTC	RT-qPCR	This study
atp2	CGCCTTGTTTCCTTGAAAGATAC	GTGCAATCTCAGCCTTCTTAAC	RT-qPCR	This study

atp18	CGTTCTTTGGCCTTAAAAGATATTC	CTTTCCAGCCTTTGGGTTTCTAG	RT-qPCR	This study
atp19	GTCGGTTTATACAATTGCAGGTCG	GCTAAGTGGCTTATTTCTTTTAAA	RT-qPCR	This study
sdh4	ACTTCCCTGCAAGAAGATTT	AGGCCAATATCATTCGTGTT	RT-qPCR	This study
cox1	GTGGTGCATACTATTGGAGT	AGAAATGTTGAGGACCGAAT	RT-qPCR	This study
cox2	TTGGGCTGTTCCTTCTTTAG	ACACCACAAAGTTCACTACA	RT-qPCR	This study
cox3	TCTTAGGAGGTCAAGCTTATG	ATACCATGAAGACCAGTAGC	RT-qPCR	This study
pcl1	CTACTTTGGCAGCACTATCT	CAATTGGAAGAACAAGCGAT	RT-qPCR	This study
isa1	CCGACAAGTTTGACGAAATA	GAGATTGCAAATCGTCATCC	RT-qPCR	This study
fip1-GSP		CAGTGTTGTTCCAACCTAGA	CLIP	This study
str1-GSP		CCGATATAGCACTTCCAACA	CLIP	This study
fio1 -830 to -741	CCCACTTCTTCCAGGCATCTG	GTCGGAGTTGGTGTCCACTTTG	ChIP-qPCR	(Jacques et al., 2014)
shu1 -179 to -80	CAATCTAGAATCAATTAGTGAGGGATAGTCTG	GCCATCTTATATAGTACTGGAAATTCAATGAATTAAG	ChIP-qPCR	(Mourer et al., 2015)
str1 -980 to -785	GTATGATCGTGTCAATGTTCTTGGCTGAAC	CTTAACTTCACTCAGATAAGATGGAGG	ChIP-qPCR	(Jbel et al., 2009)

II-5. Protein preparation & analysis

II-5.1. Protein preparation

For protein extraction, cells were lysed with ice-cold lysis buffer (50 mM Tris-Cl pH 7.5, 150 mM, NaCl, 5 mM EDTA, 10% glycerol, 1 mM PMSF, proteinase inhibitor cocktail), and glass beads. Cells were disrupted by bead beater (15 sec, 5 min break, 6 times). Cell lysates were centrifuged for 15 min at 4°C, and the supernatants were transferred to a new tube. The amount of protein was quantified using Nanodrop.

II-5.2. SDS-PAGE gel and Western blotting

Protein samples were boiled with SDS dye at 95°C and loaded on 10% or 12% SDS-PAGE gel. For western blot analysis, proteins were transferred to nitrocellulose membrane. Membranes were blocked with 5% skim milk in TBST (TBS with 1% tween-20) for 1 h and incubated with primary antibodies (1:5000) in TBST-BSA (TBST with 0.5% BSA) for 1 h. After washed with TBST for 3 times, secondary antibodies (1:5000) were treated to membrane. After 1 h incubation, membranes were washed with TBST. Target protein on the membrane was detected by chemiluminescent imaging system after treating the ECL solution.

II-6. mRNA decay assay

Cells were grown to $O.D._{600}$=0.5~1 in minimal media and then 300 ug/ml 1,10-phenanthroline was added to block transcription. Cells were harvested at the indicated time points, quickly mixed with an equal volume of -70°C ice-cold methanol to fix the cells. Total RNA was extracted from cells and cDNA was synthesized using oligo dT primers. The amount of RNA was quantified by qPCR and normalized to that of *act1*. The amount of RNA at each time point, relative to that of t=0 was plotted as a graph. Half-life of mRNA was calculated after converting the qPCR result values to $\log_2$ values.

II-7. UV crosslinking RNA-IP (CLIP)

CLIP experiment was carried out as described in (Satoh et al., 2009) with some modifications. Cells expressing FLAG-tagged protein were harvested at $O.D._{600}$=0.5~0.8 and UV crosslinked using Stratalinker (254 nm, 20,000 J/cm2 for 30 sec, 2 times). Crosslinked cells were disrupted with bead beater in lysis buffer (25 mM HEPES-KOH, pH 7.5, 150 mM KCl, 2 mM $MgCl_2$, 10 mM PMSF, 200 U/ml RNase inhibitor, 0.1% NP-40, 1 mM DTT, Protein inhibitor cocktail). Cell extracts were cleared by centrifugation at 4°C, and incubated with TURBO DNase for 30 min at 30°C. After centrifugation, the supernatant was moved to a new tube. Input samples (1% of cell extracts) were mixed with 300 ul of EB buffer (100 mM Tris-HCl pH 7.5, 150 mM NaCl, 12.5 mM EDTA, 0.1% SDS) and kept at -80°C. For immune-precipitation, cell extracts were incubated with A/G agarose (Santa Cruz) and 2 ul of anti-DDDDK-tag antibody (MBL) for 3~4 h at 4 °C. Immunoprecipitated beads were washed 4 times with wash buffer (25 mM HEPES-KOH, pH 7.5, 150 mM KCl, 2 mM $MgCl_2$). RNA was eluted by incubating beads for 5 min. at 65 °C in 150 ul of EB buffer, twice. Proteinase K was treated to the supernatants and incubated for 30 min at 42°C. at 65 °C. Equal volume of phenol:chloroform 5:1 solution was added and the supernatants were precipitated with 100% ethanol at -20°C. RNA pellets were washed with 70% ethanol and resuspended with RNase-free TDW. For qPCR analysis, cDNA was synthesized using gene-specific RT primers.

II-8. Chromatin immunoprecipitation (ChIP)

ChIP analysis was performed as described previously (Kim et al. 2020) with minor modifications. Cells were fixed with 1% formaldehyde for 15 min at RT and quenched with 125 mM glycine for 5 min. Cells were then collected, washed with TBS buffer (20 mM Tris-Cl pH 7.6, 150 mM NaCl), and were lysed with bead beater. The lysates were sonicated with 35% amplitude for 20 sec 4 times. After centrifugation for 20 min at 4 °C, the supernatant was moved to a new tube. Input samples (100 ul) were mixed with 300 ul of EB buffer [1% SDS and 250 mM NaCl in TE (100 mM Tris-Cl, 10 mM EDTA), and kept at -20 °C. Immunoprecipitation was performed with 2 ug BSA, 20 ul of A/G agarose (Santa Cruz), and 2 ul of anti-DDDDK-tag antibody (MBL) at 4°C, overnight. Immunoprecipitated beads were washed twice with TBS-T buffer and next twice with TBS buffer. DNA was extracted with 200 ul of EB buffer twice for 30 min at 65 °C. Supernatant was treated with RNase A for 1 h at 37 °C. 5 ul of Proteinase K (20 mg/ml) was treated for 2 h at 55 °C, and overnight at 65 °C. DNA was extracted through phenol extraction, followed by ethanol precipitation overnight at -20 °C. The qPCR was performed using primers presented in Table II-2. qPCR premix (Enzynomics) was used for the reaction.

II-9. Intracellular iron contents

The ferrozine-based colorimetric assay as described in (Riemer et al., 2004) was used for measuring the intracellular iron contents of fission yeast cells. 100 ul of cell lysates were mixed with 100 ul of 10 mM HCl and 100 ul of the iron-releasing reagent (a freshly mixed solution of equal volumes of 1.4 M HCl and 4.5% (w/v) $KMnO_4$ in H_2O). These mixtures were incubated for 2 h at 60 °C within a fume hood. After the mixtures had cooled to room temperature, 30 ul of the iron-detection reagent (6.5 mM ferrozine, 6.5 mM neocuproine, 2.5 M ammonium acetate, and 1 M ascorbic acid dissolved in water) was added to each tube. After 30 min, the absorbance of each sample was measured at 550 nm. The iron content of the sample was calculated by comparing its absorbance to that of a range of standard concentrations of $FeCl_3$. The intracellular iron concentration was normalized to the protein concentration of each cell extract.

CHAPTER III. RESULTS

III-1. Regulation of iron transporter mRNAs by Aco2

III-1.1. Transcriptome analysis of *aco2ΔNLS*

A previous study showed that Aco2, interacting with Chp1, has an anti-silencing effect in the heterochromatin region (Jung et al., 2019). To determine whether Aco2 would affect euchromatic gene expression as well, a genome-wide transcriptome analysis of *aco2ΔNLS* were performed via RNA-seq. Total RNAs isolated from wild-type and *aco2ΔNLS* cells were sequenced. Compared with the transcriptome of wild-type, a total of 164 protein-coding genes differentially expressed ($log_2FC>2$ or $log_2FC<-2$) in *aco2ΔNLS* were obtained: 98 genes were down-regulated and 66 genes were upregulated. Those genes were categorized by GOTermFinder (https://go.princeton.edu/cgi-bin/GOTermFinder). Analysis result of downregulated DEGs is described in Fig. III-11. The upregulated DEGs were significantly ($P<0.01$) enriched in biological process including 'transmembrane transport (GO:0055085)', 'anion transmembrane transport (GO:0098656)', 'import across plasma membrane (GO:0098739)', 'iron coordination entity transport (GO:1901678)'. To figure out which gene set is the most affected by the loss of nuclear Aco2, the list of GO terms was ranked by enrichment scores. The enrichment scores were calculated by dividing the number of genes in the list by the total number of GO categories (Fig. III-1). Based on this analysis results, the iron transporter genes including *str1*, *str3*, *shu1* were examined.

III-1.2. Expression levels of iron transporter mRNAs in *aco2ΔNLS*

In *S. pombe*, *str1*, *str3* and *shu1* are repressed under iron-sufficient condition by the iron-sensing transcription factor Fep1 (Pelletier et al., 2002; Pelletier et al., 2003) (Mourer et al., 2015). To confirm the RNA-seq results, the expression levels of those genes and other known target of Fep1 were checked by RT-qPCR. (Fig. III-2). Interestingly, RT-qPCR results revealed that *fio1*, *fip1* were significantly upregulated in *aco2ΔNLS*, in addition to *str1, str3, shu1*. These genes encode the iron-uptake proteins and their expressions are induced under iron-deficient condition. Intracellular iron concentration of *aco2ΔNLS* was similar to that of wild-type (Fig. III-3). Why is the expression of iron transport genes increased in *aco2ΔNLS?*

A

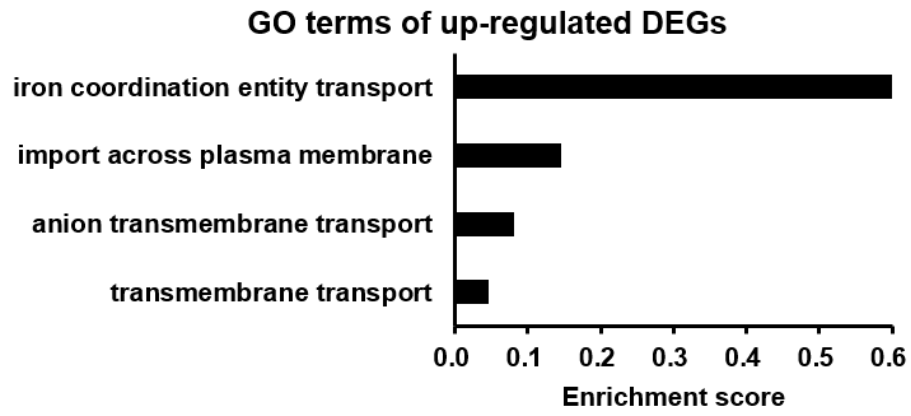

B

GO ID	GO Term	# of genes in list	Total # of genes in category	Enrichment score
GO:0055085	transmembrane transport	16	352	0.045
GO:0098656	anion transmembrane transport	8	99	0.081
GO:0098739	import across plasma membrane	7	48	0.146
GO:1901678	iron coordination entity transport	3	5	0.600

Figure III-1. GO term enrichment of upregulated genes in *aco2ΔNLS*

(A) Results of the GO term analysis using GOTermFinder (https://go.princeton.edu/cgi-bin/GOTermFinder) on significantly up-regulated genes in *aco2ΔNLS.* GO categories with $P<0.01$ are shown. The enrichment score was calculated by dividing the number of genes in list by total number of genes in GO category. (B) A list of GO term enrichment analysis

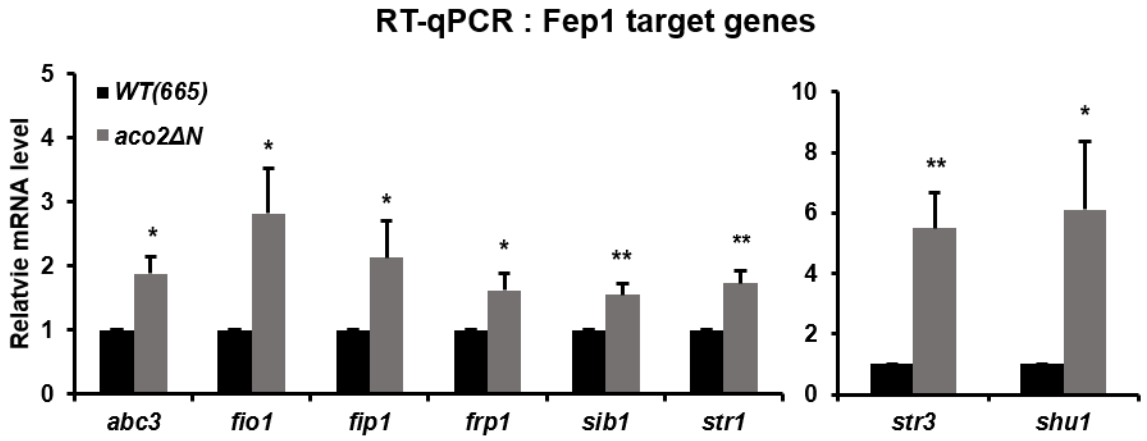

Gene	Systematic ID	Product
abc3	SPBC359.05	vacuolar heme ABC transmembrane exporter Abc3
fio1	SPAC1F7.08	plasma membrane iron transport multicopper oxidase Fio1
fip1	SPAC1F7.07c	plasma membrane iron transmembrane transporter Fip1
frp1	SPBC1683.09c	plasma membrane ferric-chelate reductase Frp1
sib1	SPAC23G3.02c	ferrichrome synthetase Sib1
str1	SPBC4F6.09	plasma membrane siderophore-iron transmembrane transporter Str1
str3	SPAC1F8.03c	plasma membrane heme transmembrane transporter Str3
shu1	SPAC1F8.02c	cell-surface heme acquisition protein Shu1

Figure III-3. Increased transcript levels of iron transporters in *aco2ΔNLS*

RT-qPCR results of iron transporter genes in wild-type and *aco2ΔNLS* cells. Relative mRNA levels of indicated genes were normalized to *act1*. Data are represented as mean (±S.E.M.) calculated from four independent experiments. *P*-values were calculated using Student's *t*-test (** $P<0.01$, * $P<0.05$).

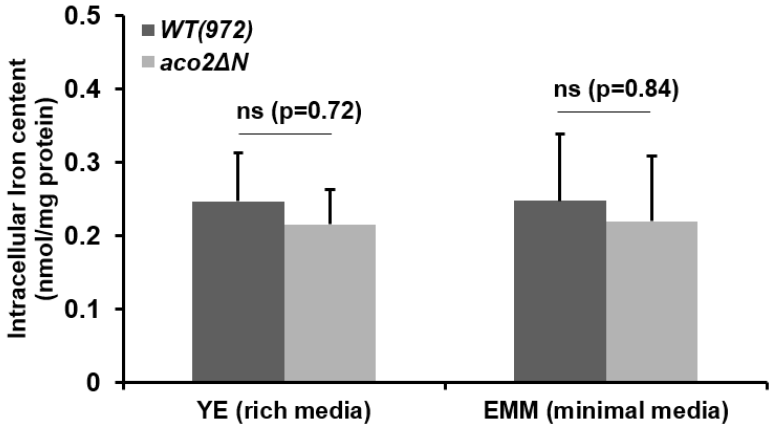

Figure III-4. Measurement of intracellular iron contents in wild-type and *aco2ΔNLS*

Cells grown in rich and minimal media were lysed and treated with acidic $KMnO_4$. Total iron content of the lysates was measured by the ferrozine method. Data represents the mean (±S.E.M.) of three independent experiments. *P*-values were calculated using two-tailed Student's *t*-test.

III-1.3. Transcription of iron transporter genes in *aco2ΔNLS*

Initially, I assumed that gene expression of Fep1 or co-repressors was decreased in *aco2ΔNLS*, resulting in upregulation of the Fep1 target genes. To verify this hypothesis, the transcription levels of Fep1 and known co-repressors (Tup11, Tup12, Php4, Fra2, Grx4) were examined by RT-qPCR (Encinar del Dedo et al., 2015; Jacques et al., 2014; Mercier et al., 2008; Pelletier et al., 2002) (Fig. III-4A). However, there was no significant difference between wild-type and *aco2ΔNLS* in the expression of iron regulators.

Next hypothesis was that the repressed gene expression by Fep1 would be partially de-repressed when Aco2 is absent in nucleus, so that expression of these mRNAs would increase. To compare the DNA binding affinity of Fep1 between wild-type and *aco2ΔNLS*, chromatin immunoprecipitation (ChIP) was performed. After ChIP, the enriched DNAs were quantified by qPCR. ChIP-qPCR result showed no difference in DNA binding affinities of Fep1 at iron transporter gene promoters between wild-type and *aco2ΔNLS* mutant (Figure III-4B). Taken together, the loss of nuclear Aco2 did not affect the transcription of iron transporter genes. Probably the reason iron transporter transcripts were increased in *aco2ΔNLS* is that these mRNAs were not properly degraded so that accumulated.

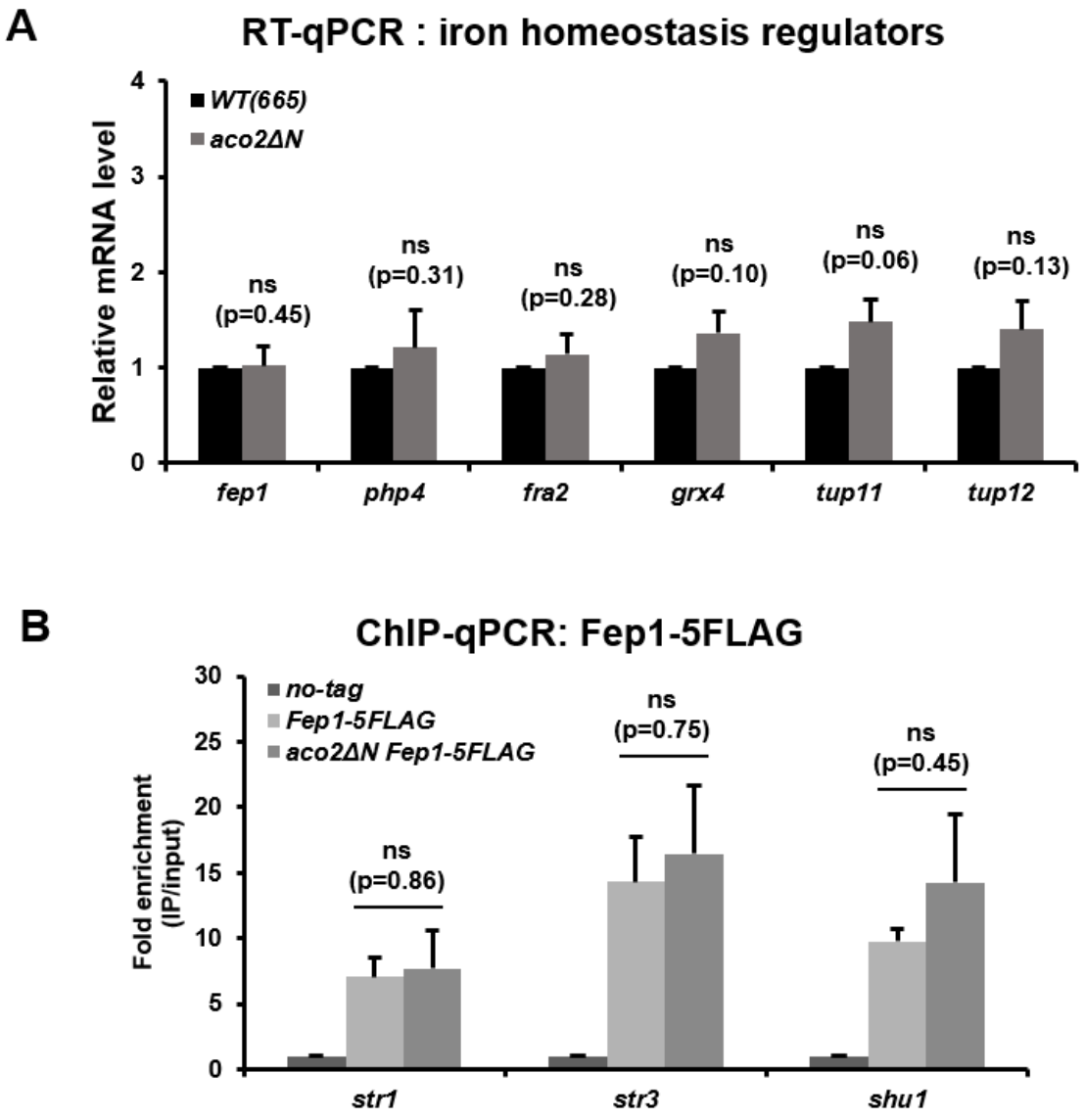

Figure III-5. Transcriptional regulation of iron transporters in *aco2ΔNLS*

(A) Transcript levels of Fep1 and co-regulators in wild-type and *aco2ΔNLS* cells. Relative expression level relative to *act1* were determined by RT-qPCR. Results are shown as the mean (±S.E.M.) calculated from three independent experiments. (B) ChIP-qPCR analysis of Fep1-5FLAG at iron transporter genes in wild-type and *aco2ΔNLS*. Fold enrichments over no-tag control are shown. All error bar indicates the S.E.M. from three independent experiments. *P*-values were calculated using Student's *t*-test.

III-1.4. Degradation of iron transporter mRNAs in *aco2ΔNLS*

To determine whether the degradation of iron transporter mRNAs was delayed in the absence of Aco2 in nucleus, mRNA decay assays were carried out. After the transcription inhibitor (1,10-phenanthroline) treatment, cells were harvested at the indicated time points and total RNA was extracted from them. The amount of mRNA was quantified by RT-qPCR (Fig. III-5A). Relative amount of mRNA at each time point, relative to t_0, was plotted. Indeed, mRNA decay rates of *fio1*, *fip1* and *str1* were significantly decreased in *aco2ΔNLS* relative to wild-type (Fig. III-5B). This data indicates that nuclear Aco2 plays a key role in mRNA degradation of iron transporters.

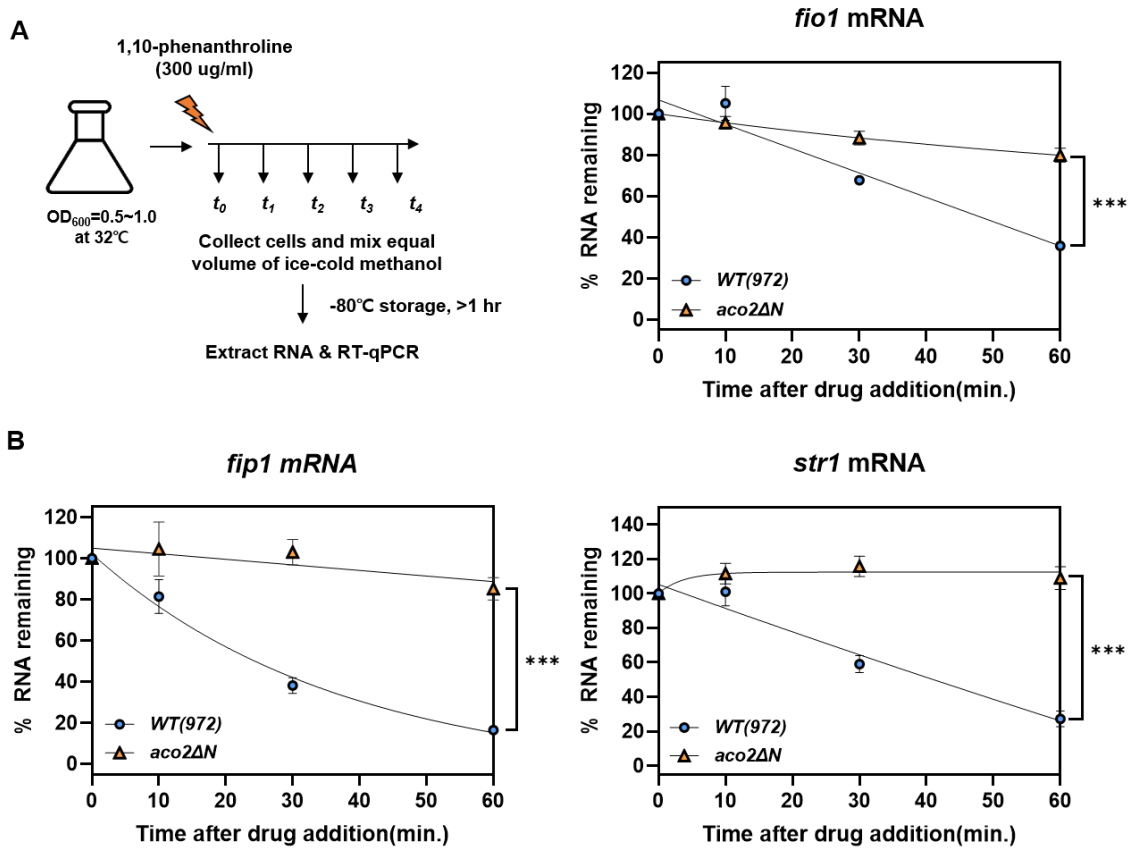

Figure III-6. Delayed degradation of iron transporter mRNAs in *aco2ΔNLS*

(A) Experimental scheme of mRNA decay assay using 1,10-phenanthroline (B) Each symbol: wild-type (blue circle), *aco2ΔNLS* (orange triangle) represents average of three independent experiments with S.E.M. (error bars). *P*-values were derived from two-tailed Student's *t*-test (*** P<0.001).

III-1.5. Aco2 domain involved in mRNA decay

Since Aco2 is consisted of two domains: aconitase domain and mitochondrial ribosomal domain (Jung et al., 2015) (Fig. I-6), I wondered which domain is required for mRNA degradation. To find the domain responsible for mRNA degradation, mRNA decay of cells expressing each domain of Aco2 in *aco2ΔNLS* was examined (Fig. III-6A).

mRNA decay of wild-type and *aco2ΔNLS* mutant were also observed as the control experiments. *aco2ΔNLS* cell showed delayed degradation of iron transporter *fio1, fip1 and str1* mRNAs (Fig. III-6B, *aco2ΔNLS).* The half-life of these mRNAs was increased by 4-6 times that of wild-type (Fig. III-6C). Surprisingly, only the aconitase domain was expressed in the nucleus, reduced degradation rates in the *aco2ΔNLS* were restored (Fig. III-6B, *aco2ΔNLS+NLS-AD*). Accumulated mRNA levels of iron transporter decreased to wild-type levels when additionally expressing the aconitase domain with NLS in *aco2ΔNLS* (Fig. III-7). On the other hand, neither expressing aconitase domain (Fig. III-7, *aco2ΔNLS+AD)* nor ribosomal domain (Fig. III-7, *aco2ΔNLS+RD) in aco2ΔNLS* was restored.

Moreover, I investigated whether the catalytic activity of Aco2 is needed when it functions in nucleus. In the case of expressing non-catalytic Aco2 whose conserved three cysteines were replaced by serine was in *aco2ΔNLS* showed the same restoring effects in *aco2ΔNLS* (Fig. III-6B; Fig. III-7, *aco2ΔNLS+aco2(3CS)*). These complementation assay results are consistent with the previous observations on telomeric RNA expression (Jung et al., 2019). Taken together, the aconitase domain is essential for the nuclear function of Aco2, and this function is possible without catalytic activity. In other words, Aco2 has the structural role in nucleus.

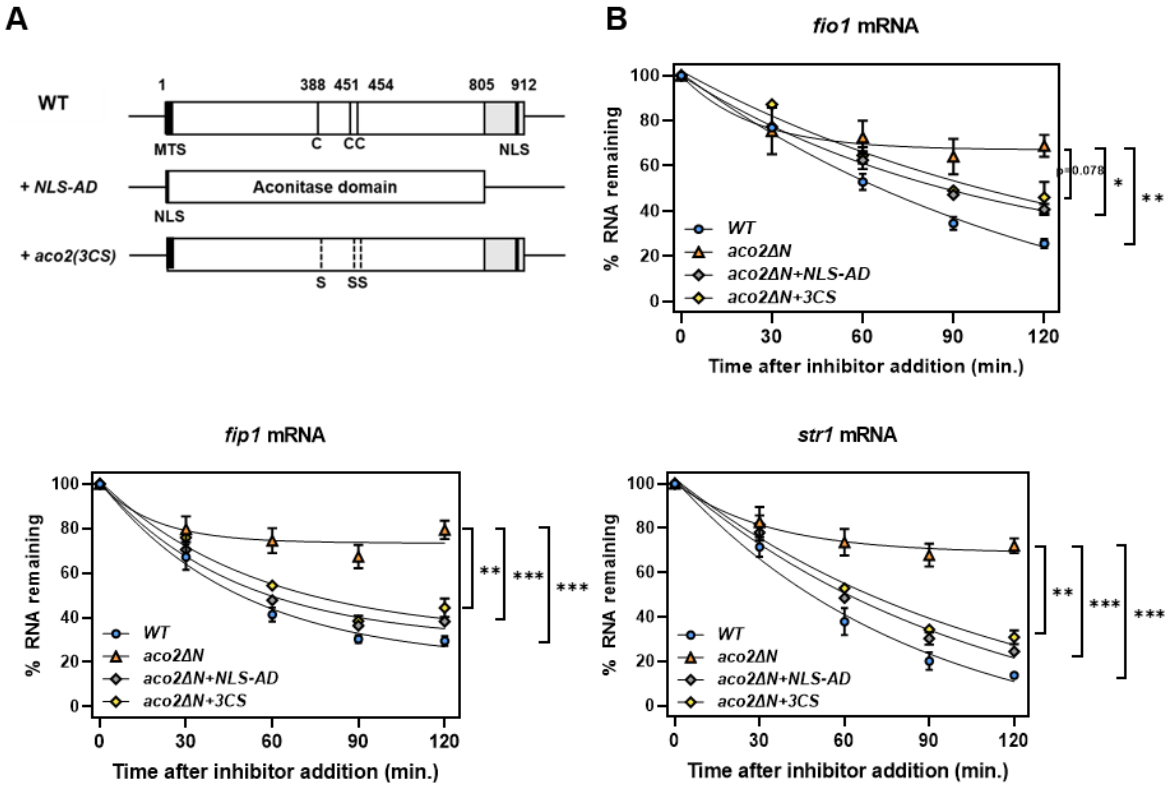

C

Half-life (h)	*fio1*	*fip1*	*str1*
WT	**1.0 ± 0.06**	**1.1 ± 0.03**	**0.7 ± 0.03**
aco2ΔN	**4.0 ± 0.63**	**5.9 ± 1.09**	**4.2 ± 0.44**
aco2ΔN+NLS-AD	**1.5 ± 0.09**	**1.3 ± 0.02**	**0.9 ± 0.04**
aco2ΔN+aco2(3CS)	**1.7 ± 0.27**	**1.5 ± 0.14**	**1.1 ± 0.09**

Figure III-7. Restoration of delayed mRNA degradation in complemented strains

(A) A schematic diagram of complemented genes. Each of them was introduced into the *leu1* site of *aco2ΔNLS* chromosome. (B) mRNA decay assay of iron transporter mRNAs in wild-type (blue circle), *aco2ΔNLS* (orange triangle), *aco2ΔNLS+NLS-AD* (gray diamond) and *aco2ΔNLS+aco2(3CS)* (yellow diamond). Each symbol represents average of three independent experiments with S.E.M. (error bars). *P*-values were derived from two-tailed Student's *t*-test (*** $P<0.001$, ** $P<0.01$, * $P<0.05$). (C) Half-life of iron transporter mRNAs in indicated strains. The mRNA half-life was calculated after converting RT-qPCR values to $\log_2$ values.

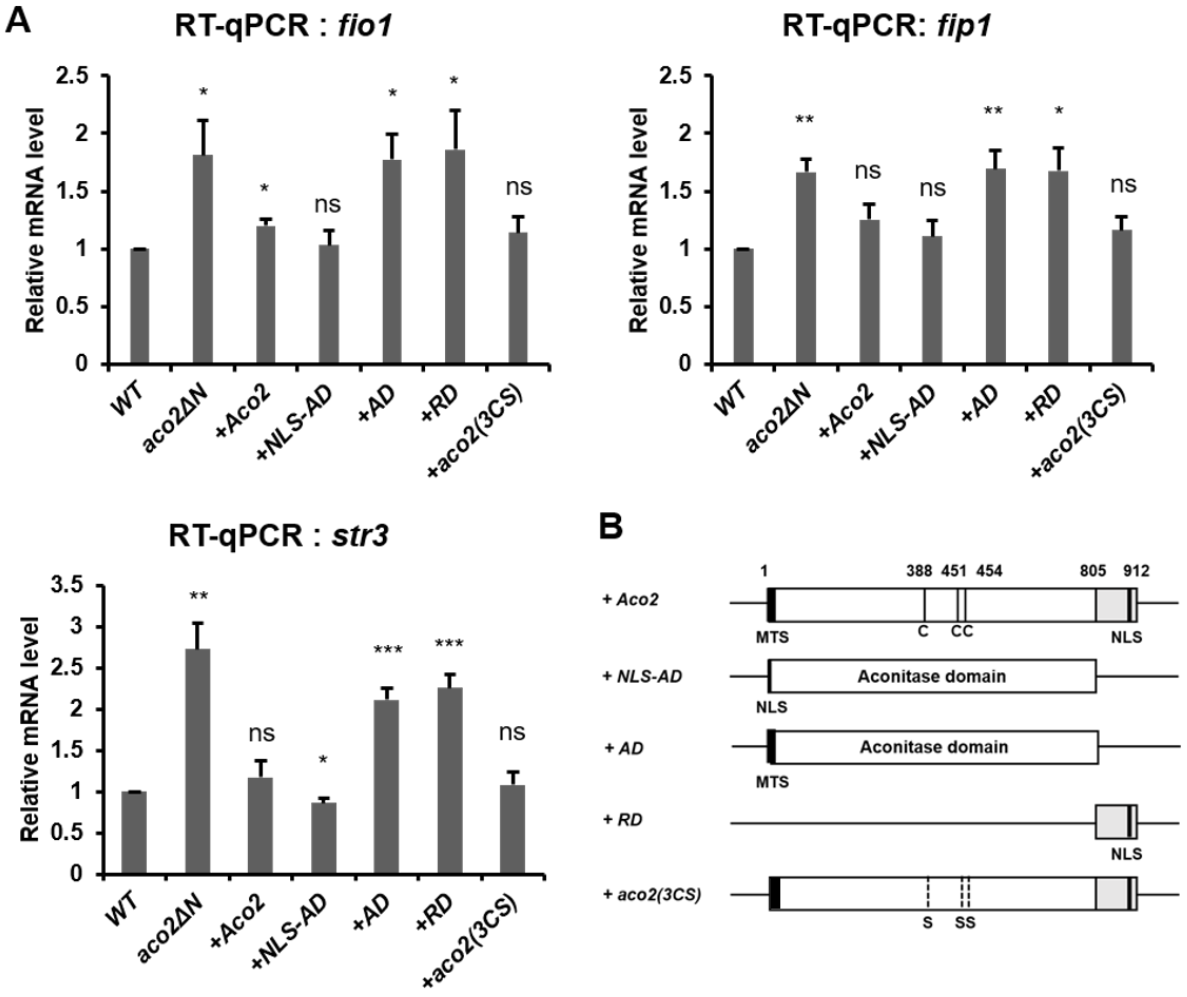

Figure III-8. Restoration of accumulated mRNAs in complemented strains

(A) Complementation analysis of *aco2ΔNLS* in which iron transporter mRNAs are accumulated. In complemented strains, the following genes were introduced into the *leu1* region of *aco2ΔNLS*: wild-type *aco2 (+Aco2)*, the aconitase domain of Aco2 with NLS (*+NLS-AD*), the aconitase domain (*+AD*), the ribosomal domain (*+RD*) and *aco2* with Cys to Ser substitution mutations of three conserved cysteines (*+aco2(3CS)*). Relative mRNA expression levels were determined by RT-qPCR. Average values from three independent experiments with S.E.M. (error bars) are shown. *P*-values compared with wild-type were obtained using Student's *t*-test (*** $P<0.001$, ** $P<0.01$, * $P<0.05$, ns $P>0.05$) (B) a schematic diagram of complemented strains described in (A).

III-1.6. RNA binding ability of Aco2

Finding that loss of nuclear Aco2 delays mRNA degradation of iron transporters suggested Aco2 is involved in mRNA decay as the RNA-binding protein. Given the conserved function of aconitase as IRP or RNA-binding proteins, *S. pombe* Aco2 is likely to bind to iron-related RNAs. I wondered whether Aco2 could bind to iron transporter mRNAs and tested this possibility using the UV crosslinking RNA-IP (CLIP) method. FLAG-tagged Aco2 cells were grown until OD_{600}=0.5~1 in minimal media and crosslinked with ultraviolet (UV). As a no-tag control, wild-type cells were used in parallel. After CLIP, cDNA was synthesized from immunoprecipitated RNA using gene-specific RT primers (*fip1*, *str1*). the enrichment level of each gene was evaluated by qPCR. In CLIP-qPCR results, *fip1* and *str1* mRNA were significantly enriched in Aco2-FLAG cells compared to no-tag control (Fig. III-8). This data indicates Aco2 binds to iron transporter mRNAs, suggesting Aco2 can serve as the mediator in mRNA degradation pathway.

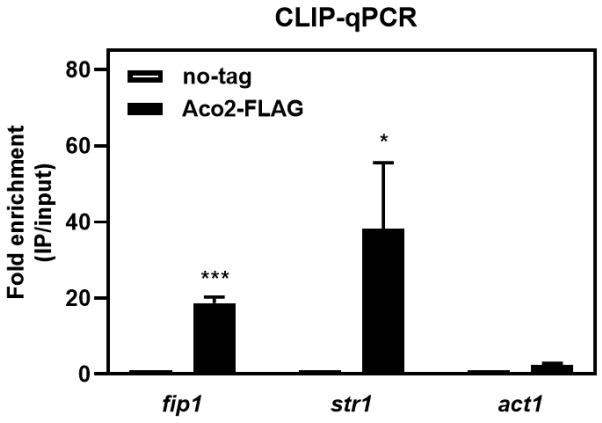

Fold enrichment over no-tag		
fip1	*str1*	*act1*
18.65 ± 1.64	38.25 ± 17.26	2.44 ± 0.47

Figure III-9. Aco2 binds to iron transporter mRNAs

Enrichments of *fip1* and *str1* mRNAs after UV crosslinking RNA-IP (CLIP) were measured by RT-qPCR. *act1* was used as a negative control. Data presented as means of fold enrichment relative to values from no-tag (WT). Error bar indicates S.E.M. from five independent experiments. Statistically significance was determined by the Student's *t*-test (*** P<0.001,* P<0.05).

III-1.6. Searching for interaction partners of Aco2

Since the post-transcriptional regulation of iron transporter mRNAs was still unknown in *S. pombe*, the mutants of ribonucleases involved in mRNA catabolic process were screened. Based on Pombase (pombase.org) annotation, the six exoribonucleases were selected: *caf1Δ*, *ccr4Δ*, *dis3-54*, *dis32Δ*, *exo2Δ* and *rrp6Δ*. At first, RT-qPCR was carried out to find the mutant in which iron transporter mRNAs were accumulated like *aco2ΔNLS*. In RT-qPCR result, accumulation of *fip1* and *str1* mRNAs was observed in following mutant candidates: *caf1Δ*, *dis3-54*, *exo2Δ* and *rrp6Δ* mutants (Fig. III-9A). Next, mRNA decay assays were performed in *caf1Δ*, *dis3-54*, *exo2Δ* and *rrp6Δ* mutants. Notably, except for *dis3-54*, delayed degradation of *fip1* and *str1* mRNAs were observed in mutant candidates (Fig. III-9B). Collectively, these results suggest that exoribonucleases such as Caf1, Exo2 or Rrp6 participate in the degradation of iron transporter mRNAs and the RNA-binding protein Aco2 is expected to act as a mediator in this mRNA decay process.

III-1.7. Interaction between Aco2 and Rrp6

A recent study reported that Aco2 was detected by affinity purification coupled with LS-MS/MS of Dis3-TAP and Rrp4-TAP, respectively (Telekawa et al., 2018). Dis3 and Rrp4 consist of RNA exosome complex together with Rrp6 (Malecki et al., 2013; Telekawa et al., 2018). Aconitase also has been reported as the component of RNA degradosome in *C. crescentus* (Fig I-5) (Hardwick et al., 2011). For these reasons, among the potential interaction partners (Caf1, Exo2 and Rrp6), Rrp6 is thought that most likely to interact with Aco2. So, genetic and physical interactions between Aco2 and Rrp6 was tested. The expression levels of *fip1* and *str1* mRNAs in *aco2ΔNLS*, *rrp6Δ* and *aco2ΔNLS rrp6Δ* double mutant were measured by RT-qPCR. The *aco2ΔNLS rrp6Δ* double mutant did not show a synergistic effect on accumulation of iron transporter mRNAs (Fig. III-10A). This data means Aco2 and Rrp6 act in the same mRNA degradation pathway. The co-IP data performed by a senior researcher in our research team also confirmed that Rrp6 is associated with Aco2 (Jung, 2016) (Fig. III-10B). In conclusion, under iron-sufficient conditions, Aco2 binds to iron transporter mRNAs and help them properly removed by the exoribonucleases like Rrp6 (Fig. III-11).

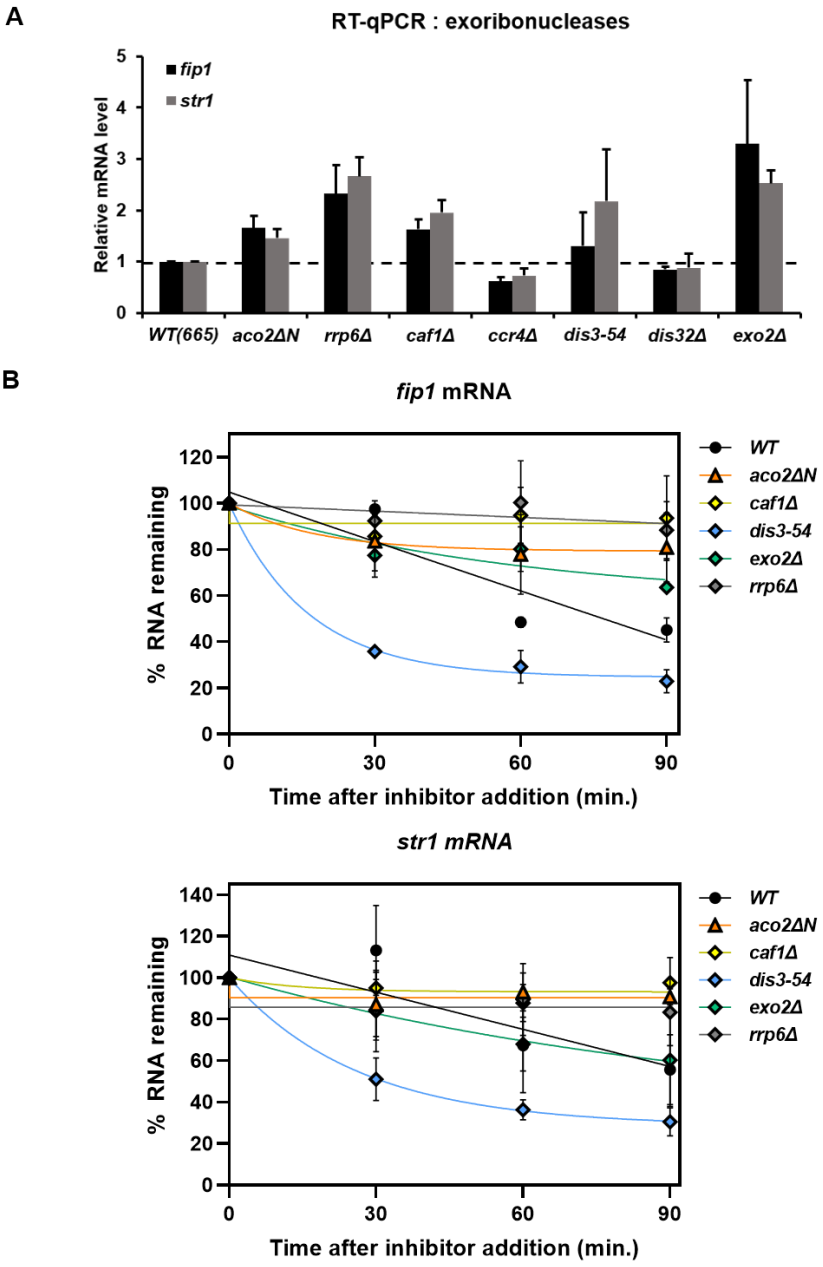

Figure III-10. Degradation of iron transporter mRNAs by exoribonucleases

(A) Relative expression levels of iron transporter mRNAs in wild-type, *aco2ΔNLS* and 6 exoribonuclease mutants were determined by RT-qPCR. Expression levels of indicated strains were normalized to *act1* mRNA and shown as the mean (±S.E.M.) from three independent experiments. (B) mRNA decay assay of *fip1* and *str1* mRNAs in wild-type (black circle), *aco2ΔNLS* (orange triangle), *caf1Δ* (yellow diamond), *dis3-54* (blue diamond), *exo2Δ* (green diamond) and *rrp6Δ* (gray diamond). Each symbol represents average of two independent experiments with S.E.M. (error bars).

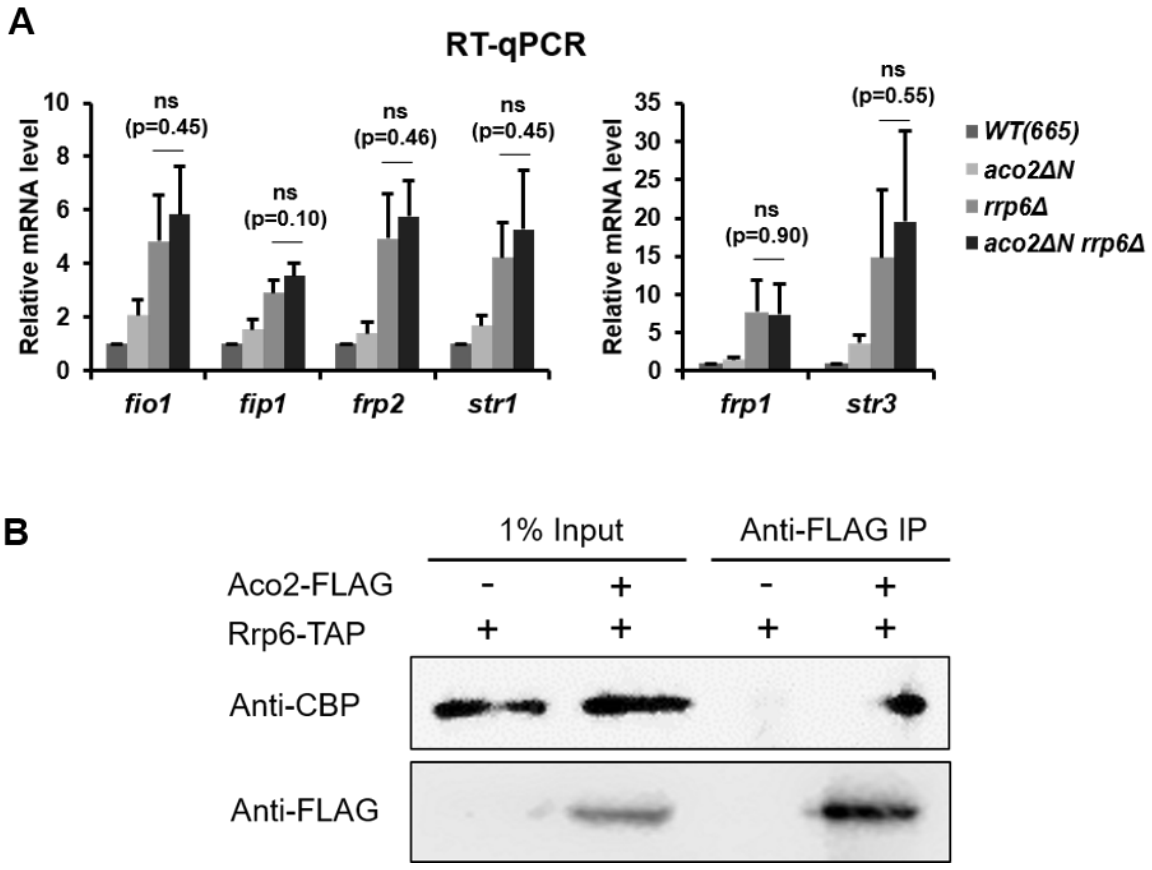

Figure III-11. Genetic and physical interactions between Aco2 and Rrp6

(A) RT-qPCR analysis of iron transporter mRNAs in WT, *aco2ΔNLS*, *rrp6Δ* and *aco2ΔNLS rrp6Δ* cells. Results are shown as the mean (±S.E.M.) calculated from three independent experiments. *P*-values were calculated using Student's *t*-test. (B) Co-IP analysis of Aco2 and Rrp6 interactions. Whole cell lysates from Aco2-FLAG and Rrp6-TAP expressing cells were subjected to immunoprecipitation with anti-FLAG antibody. Western blot analysis of cell lysates before (input) and after FLAG-IP is shown (Jung, 2016).

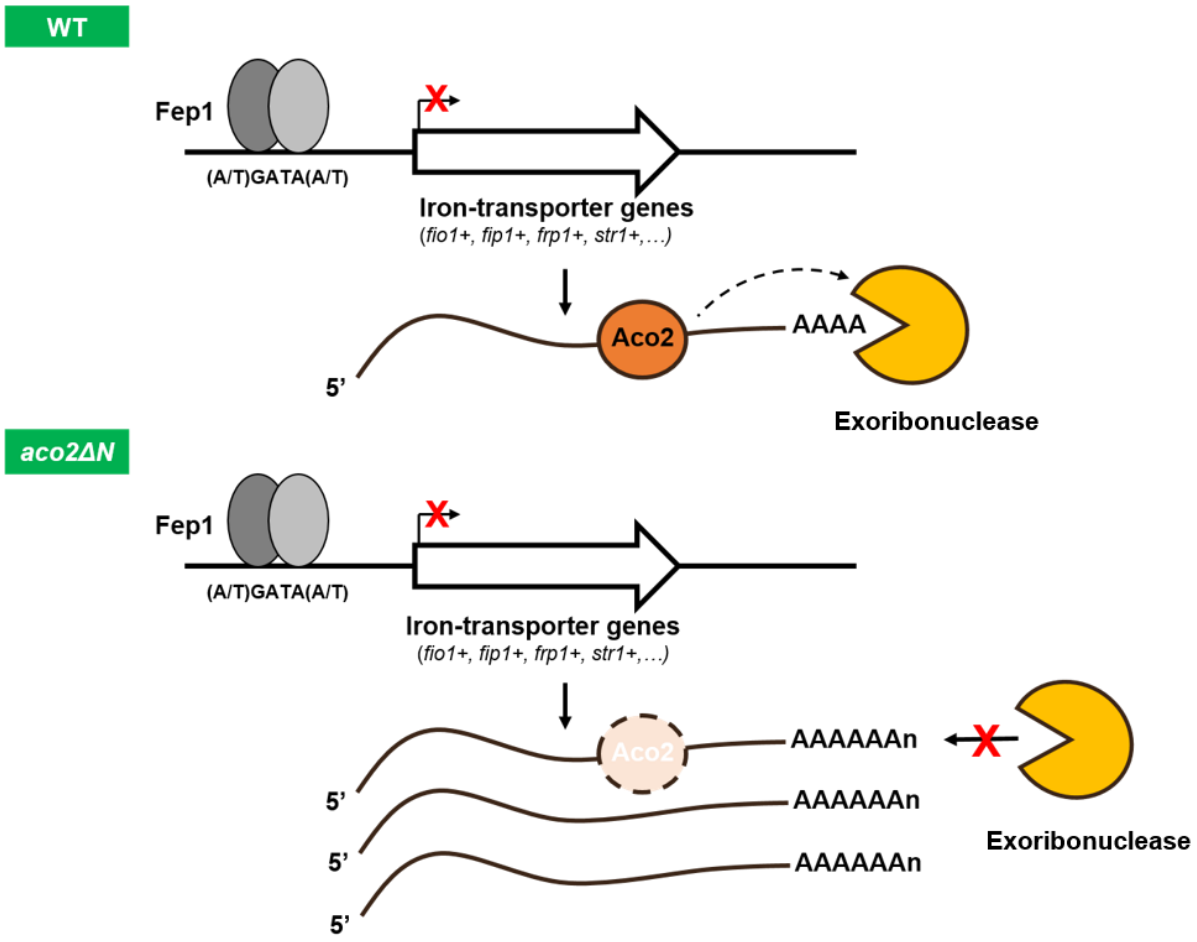

Figure III-12. Aco2-mediated post-transcriptional regulation of iron transporters

Under iron-sufficient conditions, unnecessary iron-uptake mRNAs are removed by the exoribonucleases. Aco2 mediates this mRNA decay process as the RNA-binding protein. In the absence of Aco2, iron transporter mRNAs are poorly degraded and accumulated in cells.

III-2. Regulation of nuclear-encoded ETC genes by Aco2

III-2.1. Comparison of cell growth in different media

To determine the effect of nuclear Aco2 loss on cells, the basic phenotypes of *aco2ΔNLS* were investigated. Growth curves of wild-type and *aco2ΔNLS* cells in rich and minimal media were analyzed (Fig. III-12). Cells grown in rich media showed little difference in growth rate or final O.D. value. However, the growth rate of *aco2ΔNLS* cells in minimal media was decreased and final O.D. was lower than that of wild-type. Since EMM minimal media demands the respiratory growth than YE rich media (Malecki et al., 2016), *aco2ΔNLS* cells were considered that had a problem with cellular respiration. To clarify this assumption, cell growth on media containing 0.1% glucose was observed (Fig. III-13A). 0.1% glucose is known as the critical concentration for respiratory-dependent proliferation (Takeda et al., 2015). The growth rate of *aco2ΔNLS* cells in 0.1% glucose media was decreased and final O.D. was lower than that of wild-type. Furthermore, cell growth on media containing non-fermentable carbon sources was observed by spotting assay (Fig. III-13B). The fission yeast use respiration rather than fermentation in media containing galactose or glycerol (Malecki et al., 2016). *aco2ΔNLS* displayed a growth defect in nonfermentable carbon source media. This data indicates that loss of Aco2 in nucleus leads to inhibition of cellular respiration.

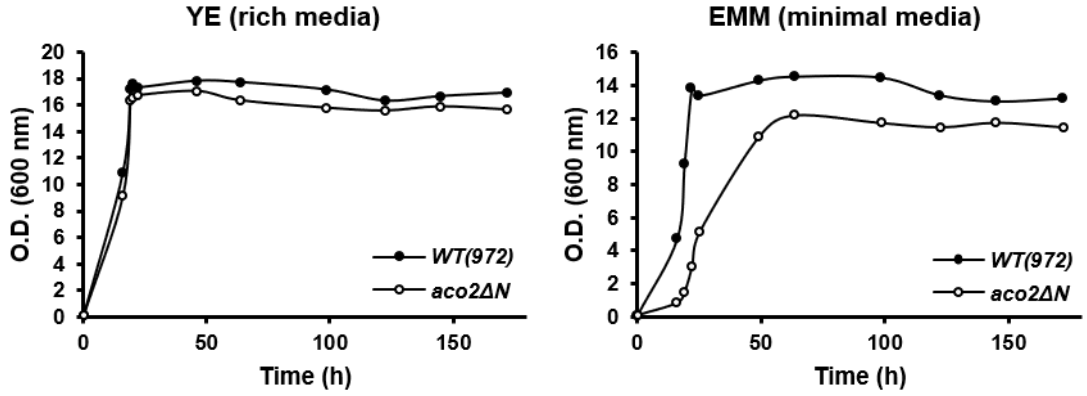

Figure III-13. Growth curve analysis of wild-type and *aco2ΔNLS* cells

A Growth curve of wild-type and *aco2ΔNLS* in YE and EMM media. Cells were grown in indicated media for ~180 hours with shaking at 180 rpm, 30°C. The O.D. (optical density) of cells were measured at 600 nm (initial O.D.=0.1).

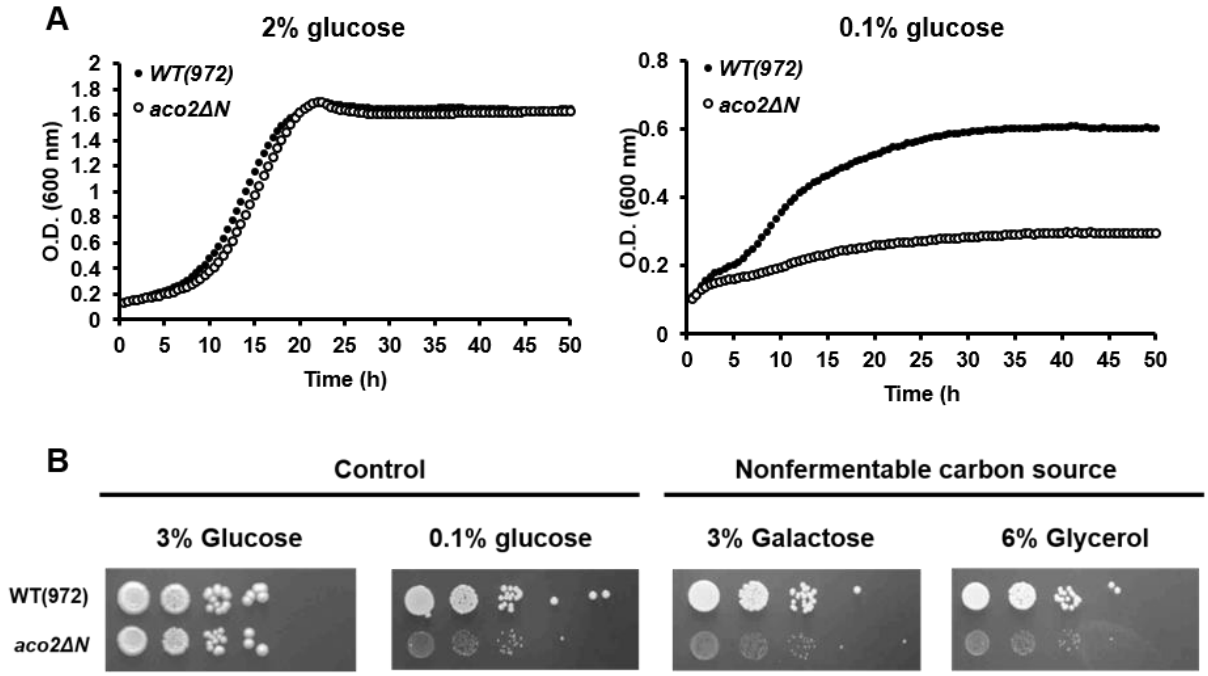

Figure III-14. Respiratory growth defect of *aco2ΔNLS*

(A) Automatic growth monitoring by microplate reader Tecan. Cells were grown in minimal media with 2% (EMM) or 0.1% glucose with initial O.D.=0.1. The O.D. at 600 nm was measured every 30 minutes for about 50 hours. (B) Spotting assay on rich media containing indicated carbon sources. A serial 10-fold dilutions of liquid cultures were spotted onto plates and plates were incubated at 32°C for 4 days. The composition of nonfermentable carbon source media is as follow: YE media with 0.1% glucose and 3% galactose; YE media with 0.1% glucose and 6% glycerol.

III-2.2. Transcriptome analysis of downregulated genes in *aco2ΔNLS*

To figure out how the loss of nuclear Aco2 have a physiological effect on cells, the RNA-seq result was analyzed. Compared to wild-type, downregulated ($log_2FC<-1.5$) 313 protein-coding genes were categorized by GOtermFinder. Significantly ($P<0.01$) enriched GO terms in biological process are displayed in Fig III-14. Interestingly, most of GO terms were related to oxidative phosphorylation.

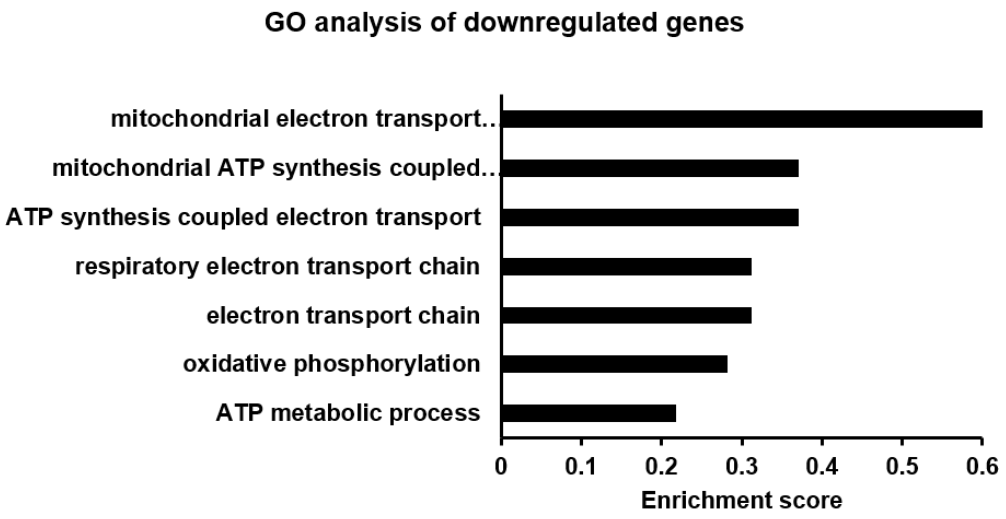

GO ID	GO Term	# of genes in list	Total # of genes in category	Enrichment score
GO:0006122	mitochondrial electron transport, ubiquinol to cytochrome c	6	10	0.60
GO:0042773	ATP synthesis coupled electron transport	10	27	0.37
GO:0042775	mitochondrial ATP synthesis coupled electron transport	10	27	0.37
GO:0022900	electron transport chain	10	32	0.31
GO:0022904	respiratory electron transport chain	10	32	0.31
GO:0006119	oxidative phosphorylation	13	46	0.28
GO:0046034	ATP metabolic process	15	69	0.22
GO:0008150	biological_process	74	734	0.10
	unannotated	13	40	0.60

Figure III-15. GO term enrichment of downregulated genes in *aco2ΔNLS*

GO terms of downregulated genes in *aco2ΔNLS* were analyzed and ranked by enrichment score. (Enrichment score = # of genes in list / total # of genes in GO category)

Transcript levels of electron transport chain (ETC) genes were confirmed by RT-qPCR. Expression of nuclear-encoded ETC genes, especially included in complex III (*qcr2*, *qcr9*), IV (*cox9*, *cox13*) and V (*atp2*, *atp18*, *atp19*) were decreased in *aco2ΔNLS.* Mitochondrial-encoded ETC genes (*cox1*, *cox2*, *cox3*), on the other hand, were no significant difference in their expression (Fig. III-15).

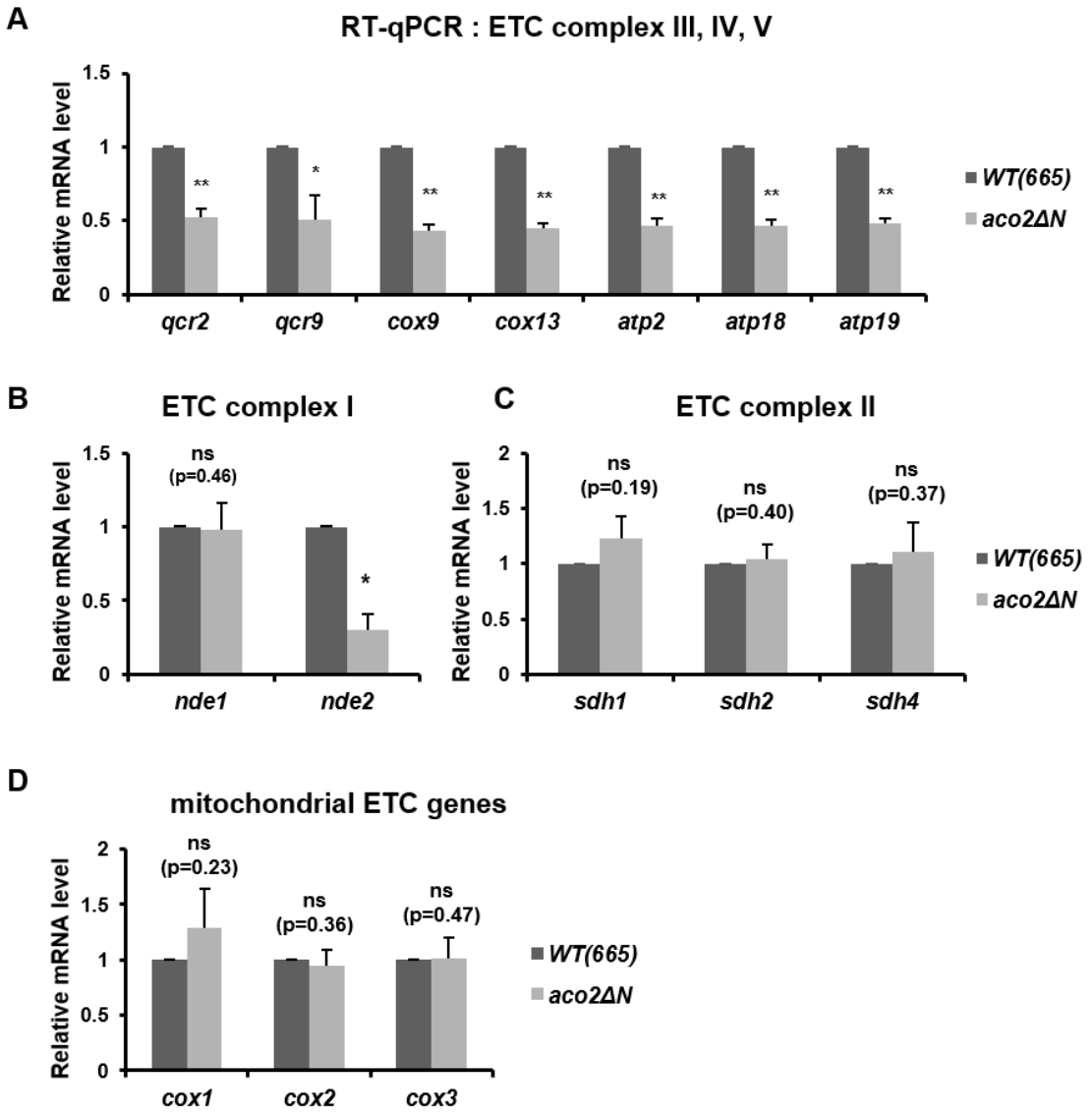

Figure III-16. Expression of electron transport chain (ETC) genes in *aco2ΔNLS*

(A-C) RT-qPCR results of nuclear-encoded ETC genes (A-C) and mitochondrial-encoded ETC genes (D). Data are represented as mean (±S.E.M.) calculated from three independent experiments. *P*-values were calculated using Student's *t*-test (** $P<0.01$, * $P<0.05$).

III-2.3. Transcription of nuclear-encoded ETC gene regulators

Since expression of nuclear-encoded ETC genes was decreased overall, I wondered if the expression of transcription factors regulating these genes would be affected by the loss of nuclear Aco2. In *S. pombe*, regulatory mechanism of ETC gene expression has not been elucidated yet. So, transcription levels of Php complex, homologs of the HAP complex in budding yeast, were examined instead. The HAP complex is known as a master regulator of respiratory metabolism. It binds to the CCAAT sequence in the upstream activation sequence (UAS) of cytochrome genes, similar to its role in the mammalian cells (Mao and Chen, 2019). RT-qPCR results exhibited no change in the expression of Php2/Php3/Php5 (Fig. III-16) and Php4 genes (Fig. III-4A).

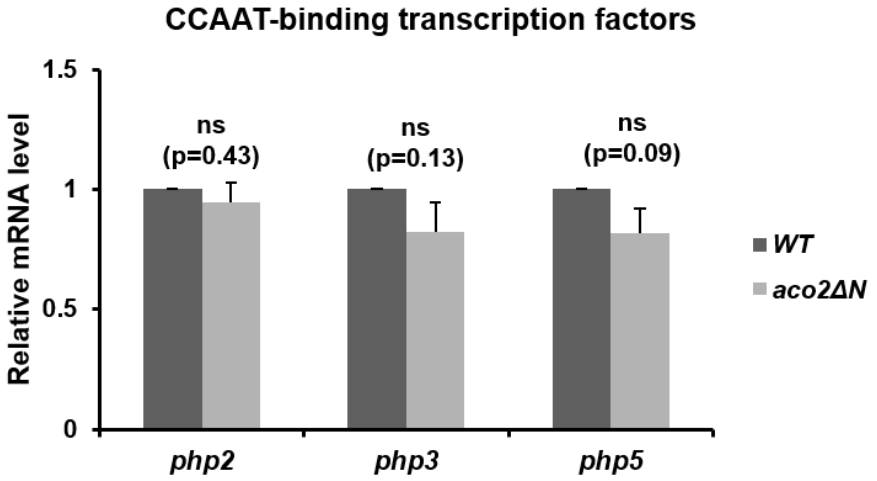

Figure III-17. Transcription of CCAAT-binding Php complex

Relative expression levels of CCAAT-binding Php complex genes were measured by RT-qPCR and normalized to that of *act1* mRNA. Data indicates the mean value (±S.E.M.) calculated from three independent experiments. *P*-values were calculated using Student's *t*-test.

III-2.4. mRNA stability of nuclear-encoded ETC genes

In my previous experiment, I found out Aco2 participates in the mRNA degradation process. I thought that Aco2 might affect the degradation of ETC genes, so that observed mRNA decay of nuclear-encoded ETC genes (Fig. III-17). *qcr2*, *cox7*, and *atp2* mRNAs were used to represent ETC complexes III, IV and V, respectively. The mRNA decay was measured by RT-qPCR following transcription inhibition using 1,10-phenanthroline. The amount of each mRNA was normalized to *act1* mRNA and quantified by RT-qPCR. Unexpectedly, *qcr2*, *cox7* and *atp2* mRNAs were stable in both wild-type and *aco2ΔNLS*. Only the amount of these mRNAs in *aco2ΔNLS* was lower than wild-type, corresponding to the RT-qPCR result on Fig. III-15.

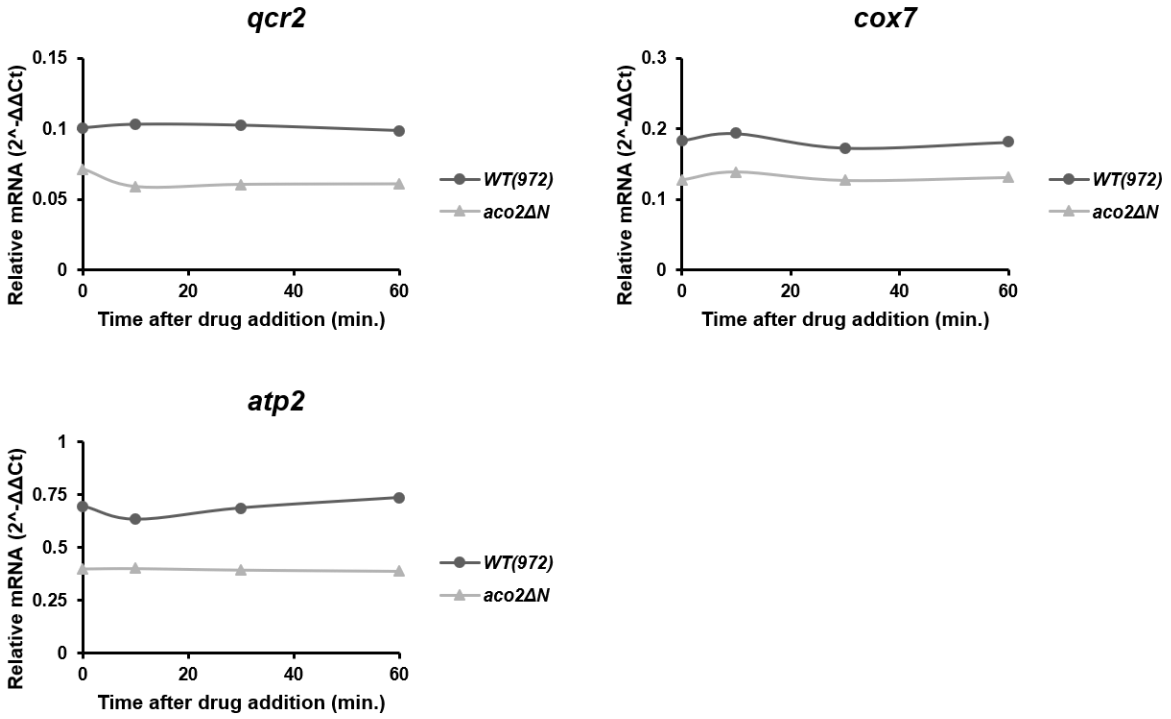

Figure III-18. Analysis of ETC mRNA stability with transcription inhibitor

The trace of *qcr2*, *cox7* and *atp2* mRNAs after 1,10-phenanethroline (300 ug/ml) treatment. RT-qPCR data were analyzed by the 2^-*ΔΔ*Ct method for displaying the amount of RNA remaining in the cell.

III-2.5. Analyzing expression of ETC proteins

As the expression of nuclear-encoded ETC genes in *aco2ΔNLS* decreased, the amount of protein was expected to decrease. The amount of Qcr2 (ETC complex III) and Cox13 (ETC complex IV) protein were estimated by western blot analysis. FLAG-tagged Qcr2 or Cox13 from whole cell lysates were detected by anti-FLAG antibodies. The relative amount of proteins in SDS-PAGE gel bands were quantified using Image J. The results of western blot analysis were showed that expression of Qcr2 and Cox13 proteins was reduced in *aco2ΔNLS* (Fig. III-18), elucidating why cellular respiration is inhibited in *aco2ΔNLS* mutant.

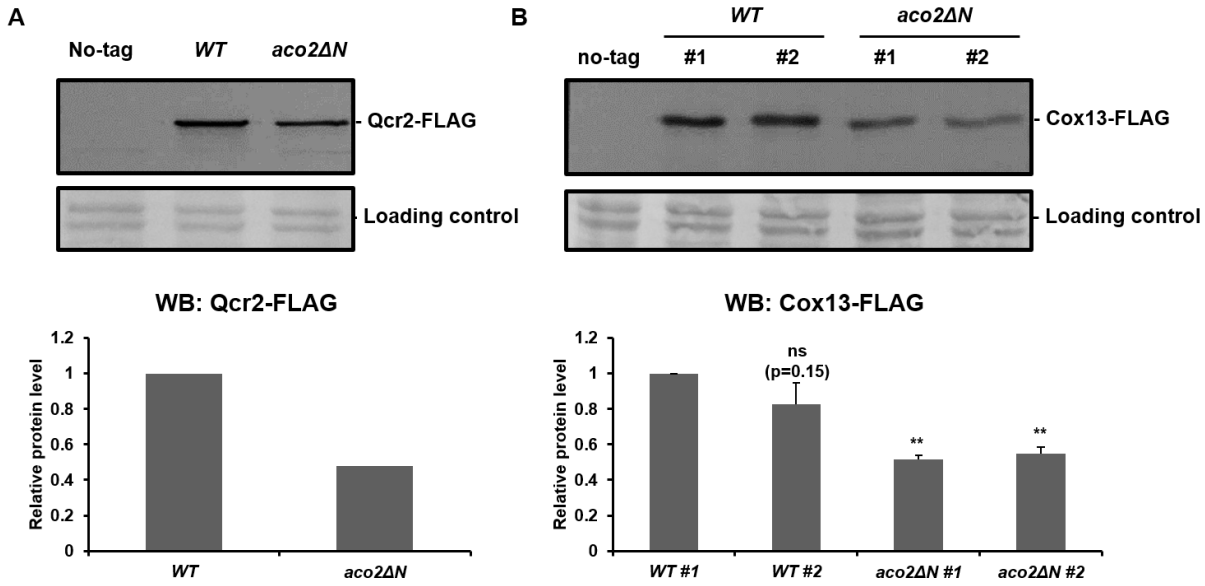

Figure III-19. Decreased protein expression of Qcr2 and Cox13 in *aco2ΔNLS*

Western blot analysis of Qcr2-FLAG (A) and Cox13-FLAG (B) proteins in wild-type and *aco2ΔNLS.* Cells expressing FLAG-tagged Qcr2 or Cox13 were grown in EMM minimal media. Whole cell lysates were loaded in 12% SDS-PAGE gel. After western blotting, the gel band of each FLAG-tagged protein was quantified by Image J and normalized to that of loading control. (A) A bar graphs shows fold change over wild-type. (B) A bar graph shows the mean value of fold change over wild-type #1. Error bars indicate ±S.E.M. from three independent experiments. *P*-values were determined by using Student's *t*-test (** $P< 0.01$).

III-2.6. Aco2 domain required for nuclear-encoded ETC gene regulation

It has been found that Aco2 requires the aconitase domain to act in iron transporter mRNA degradation and its catalytic activity is not essential (Fig. III-6; Fig. III-7). Are the aconitase domains important when playing a role in regulating ETC genes? Complementation assay revealed that aconitase domain with NLS has the same restored effect on the ETC gene regulation (Fig. III-19). Decreased transcript levels of *qcr2,* used *cox7* and *atp2* were elevated to the level of wild-type when expressing NLS-AD to the *leu1* site of *aco2ΔNLS* (Fig. III-19A). In the case of expressing non-catalytic Aco2 to *aco2ΔNLS* cells, transcript levels of ETC genes were also increased. On the contrary, when expressing the aconitase domain or ribosomal domain, the transcript levels were still reduced.

Likewise, the growth defect of *aco2ΔNLS* on the nonfermentable carbon source media was overcame by expressing aconitase domain to nucleus or non-catalytic Aco2 (Fig. III-19B). Expression of only the ribosomal domain could not overcome the growth defect of the mutant. As a result, the aconitase domain of Aco2 is essential for ETC gene regulation, it is possible without catalytic activity. Presumably, the reason that *S. pombe* Aco2 has an additional ribosomal domain is to send the aconitase domain to the nucleus so that it can be involved in the regulation of gene expression.

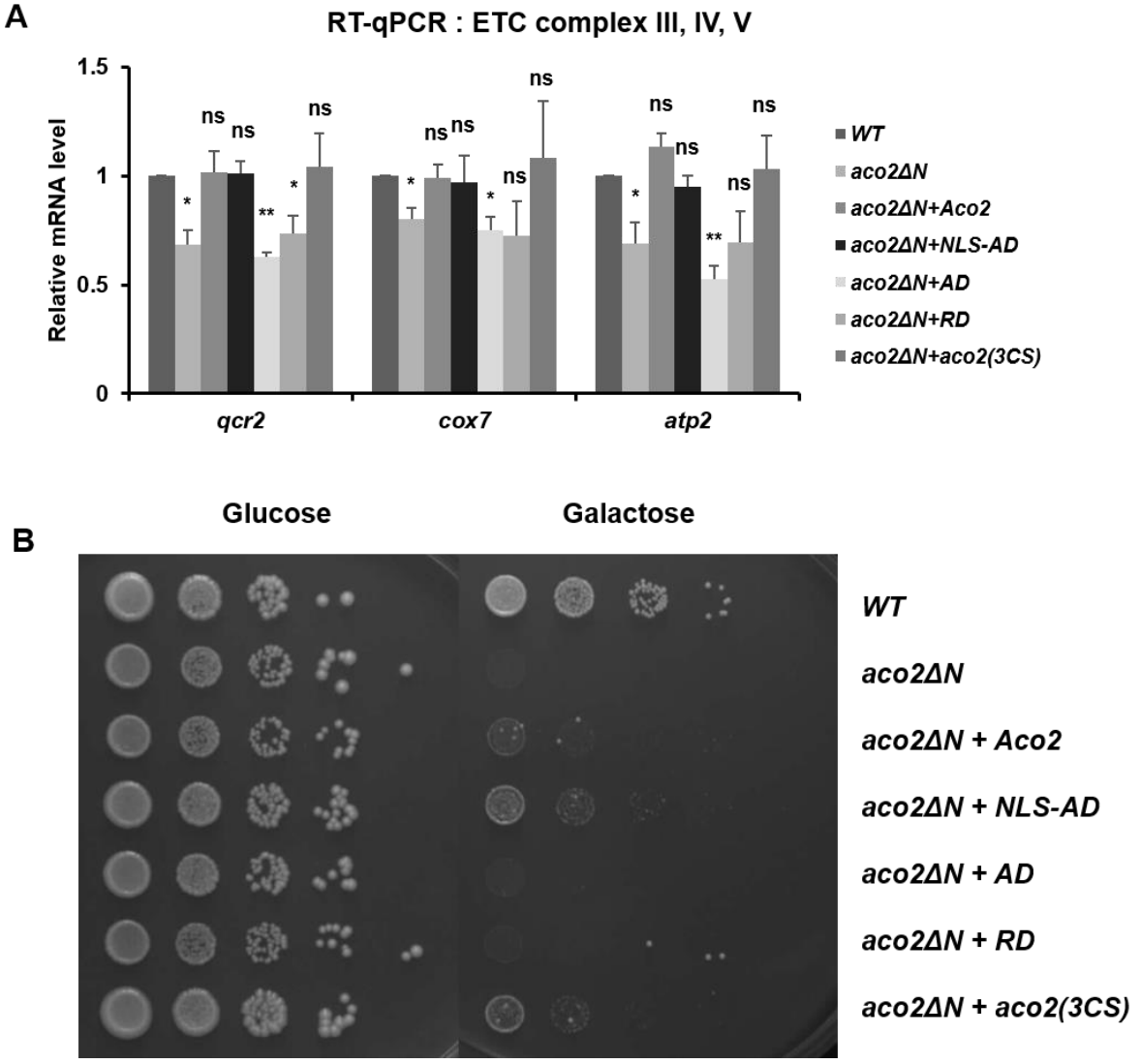

Figure III-20. Restoration of respiratory growth defect in complemented strains

(A) RT-qPCR results of complemented strains. The following genes were introduced into the *leu1* region of *aco2ΔNLS*: wild-type *aco2 (+Aco2)*, the aconitase domain of Aco2 with NLS (*+NLS-AD*), the aconitase domain (*+AD*), the ribosomal domain (*+RD*) and *aco2* with Cys to Ser substitution mutations of three conserved cysteines (*+aco2(3CS)*). Data represented as the mean (±S.E.M.) calculated from three independent experiments. Statistically significance was determined by the Student's *t*-test (** $P<0.01$, * $P<0.05$, ns $P>0.05$). (B) Spotting assay on minimal media containing glucose or galactose as a carbon source. A serial 10-fold dilutions of liquid cultures were spotted onto plates and plates were incubated at 32°C for days. The composition of galactose media is EMM media with 0.1% glucose and 3% galactose. As a control, EMM media with 2% glucose was used.

CHAPTER IV. DISCUSSION

IV-1. Degradation mechanism of iron transporter mRNA

In this study, I demonstrated that the fission yeast Aco2 is involved in iron homeostasis by mediating the degradation of iron transporter mRNAs. I showed that Aco2 can bind to iron transporter mRNAs and interact with exoribonucleases, suggesting that nuclear Aco2 plays a post-transcriptional regulatory role of iron transporters.

However, the interaction between Aco2 and exoribonucleases other than Rrp6 is still unclear. Although I proposed Caf1, Exo2 and Rrp6 as the candidates, the interactions with them or other ribonucleases in *S. pombe* need to be explored further. The physical interaction between Rrp6 and Aco2 was confirmed (Fig. III-10B), but I doubt whether these iron transporter mRNAs are degraded by Rrp6. A recent study showed that Rrp6 provides the structural role in the degradation of iron-related mRNAs (Mukherjee et al., 2016). By comparing the genome-wide transcript levels in *rrp6Δ* mutant to those in non-catalytic *rrp6* mutant, they found the "protein-dependent" target mRNAs of Rrp6. Iron transporter genes like *fio1*, *fip1*, *frp1*, *sib1*, *str1* and *str3* were included in that list, all of which were accumulated in *aco2ΔNLS*. I suspected that Aco2 will bind to these iron-related mRNAs and lead them to the exosome using Rrp6 as an adapter, so that Dis3 finally degrades these mRNAs. But, in the result of mRNA decay assay (Fig. III-9), *dis3-54* mutant showed the normal degradation pattern similar to wild-type, indicating Dis3 does not participate in this degradation pathway. Perhaps other ribonucleases rather than RNA exosome will be involved in the degradation of iron transporter mRNAs.

IV-2. Specific recognition of iron transporter mRNAs by Aco2

In that involved in iron homeostasis as the RNA-binding protein, the fission yeast Aco2 acts similarly to the iron-regulatory protein (IRP), although its protein sequence is more similar than that of mitochondrial aconitase (Fig. IV-1). Like IRP, *S. pombe* Aco2 is thought to bind to iron transporter mRNAs by recognizing a specific sequence. I first searched the iron-responsive elements (IREs) on eight target mRNAs of Aco2 described in Fig. III-2 using the SIREs Web Server 2.0 (Iron Responsive Elements Prediction Server, http://ccbg.imppc.org/sires). Except *fio1*, no IRE was predicted on target mRNAs (Fig. IV-2).

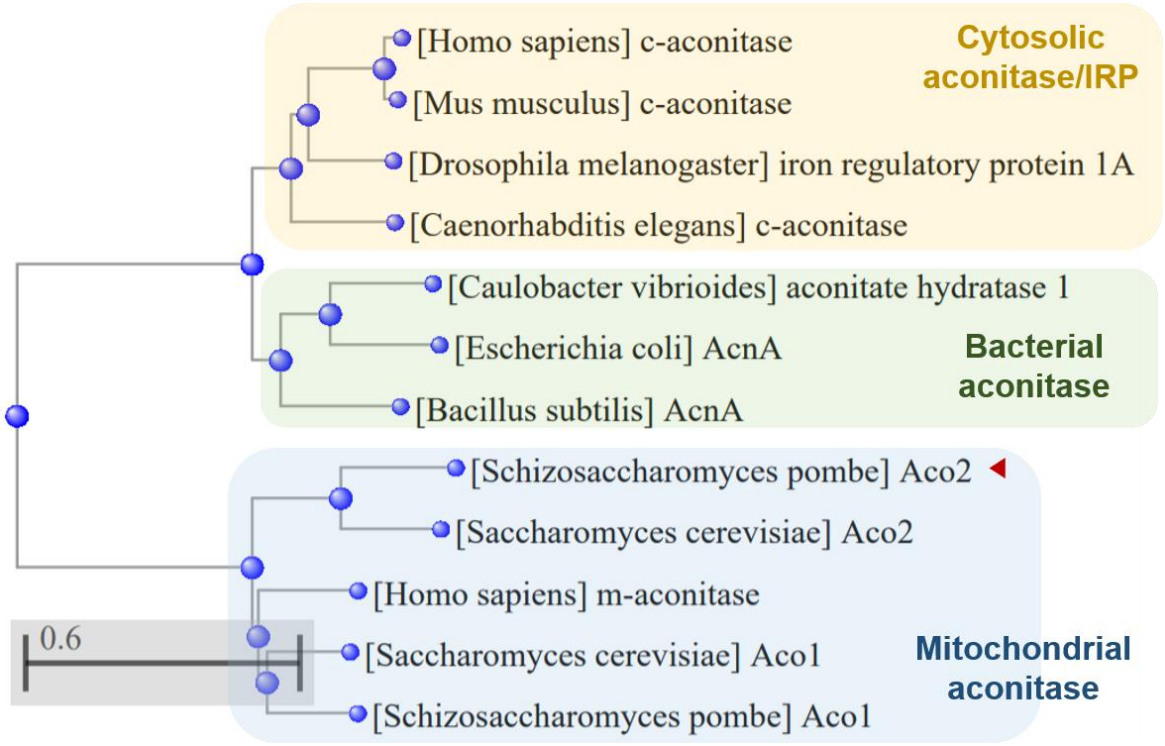

Figure IV-1. A phylogenetic tree of aconitase in various model organisms

The aconitase protein sequences in each organism were obtained from NCBI and aligned using COBALT (Constraint-based Multiple Alignment Tool).

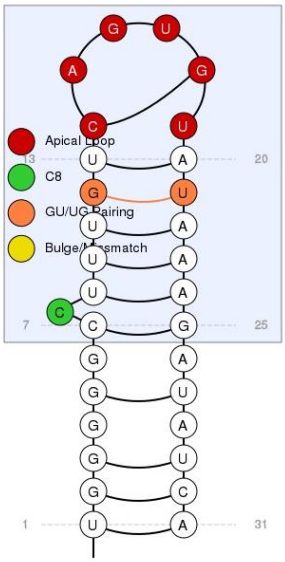

Figure IV-2. The predicted IRE on the *S. pombe fip1* mRNA

The SIREs Web Server 2.0 (Iron Responsive Elements Prediction Server) searched the IRE on *S. pombe fip1* mRNA. mRNA sequence of *fip1* used as an input was obtained from NCBI.

Furthermore, the common sequences between 8 iron transporter mRNAs were searched by the MEME suite (http://meme-suite.org), an online tool for the discover and analysis of sequence motif, to find the binding motif of Aco2. The input sequence of each mRNA was obtained from NCBI Reference Sequence. MEME reported the three of the highest scoring motifs, which were U- or GU-rich sequences (Fig. IV-3).

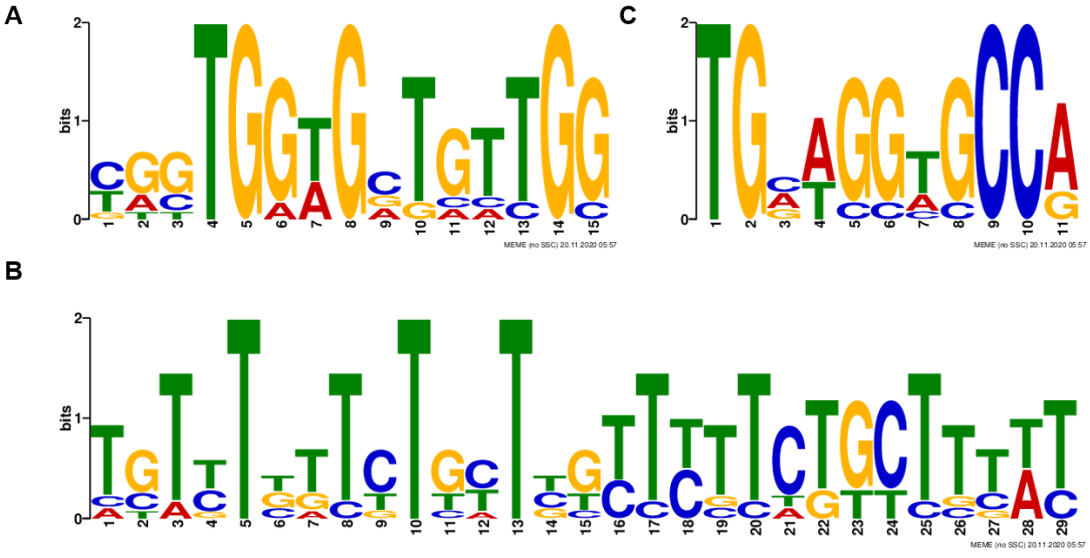

Figure IV-3. Sequence logos of the motifs identified using the MEME search tool

E-value of each motif is as follow: (A) 2.22e+0.022, (B) 1.4e+0.004 (C) 2.3e+004

Along with the AAUAAA element, the GU-rich elements are recognized by protein factors involved in the polyadenylation and mRNA 3’ end processing (Davis and Shi, 2014). Notably, the GU-rich element (GRE) was identified as a conserved sequence enriched in the 3' UTR of human transcripts that exhibited rapid mRNA turnover (Vlasova-St Louis and Bohjanen, 2011). This corresponds to my experimental results showing that Aco2 regulates the expression of iron transport genes by mediating their mRNA degradation. Among the potential interaction partners of *S. pombe* Aco2 (Fig. III-9), the Caf1 has a poly(A)-specific ribonuclease activity (Jonstrup et al., 2007). It is possible that Aco2 interacts with Caf1.

IV-3. Transcriptional regulation of nuclear-encoded ETC genes by Aco2

In *S. pombe,* certain mechanisms that regulate the expression of nuclear-encoded ETC genes have not been identified. So, it was more difficult to understand how Aco2 is involved in the expression of these genes. However, some experimental results showed that Aco2 will regulate these genes at the transcription level: most of gene expression of nuclear-encoded ETC in *aco2ΔNLS* were decreased (Fig. III-15) and there was no difference between wild-type and *aco2ΔNLS* in the degradation rate of ETC mRNAs (Fig. III-17). Loss of Aco2 in nucleus did not affect the transcription levels of Php complex (Fig. III-16), but might weaken the CCAAT binding activities of Php2/3/5 on promoter regions of ETC genes. Whether the DNA binding activity of Php2 is dependent on the presence or absence of Aco2 in the nucleus can be confirmed by ChIP experiments.

On the other hand, it might be possible that Aco2 itself can act like a transcription factor. Indeed, yeast aconitase has been reported that binds to mitochondrial DNA (Chen et al., 2005), the fission yeast Aco2 could bind the promoter regions of nuclear-encoded ETC genes and regulate their expression. This hypothesis also can be proved by ChIP.

IV-4. Mechanisms of dual targeting of Aco2

S. pombe Aco2 has a unique feature that locates in mitochondria, cytosol and nucleus. Alternative termination makes the long transcript containing NLS in ribosomal domain and only Aco2 translated from the long transcript has a dual targeting property (Fig. I-7) (Jung et al., 2015). I tried to find the environmental conditions for generating more long form of *aco2* transcripts. Since Aco2 is involved in the maintenance of iron homeostasis, I wondered if the iron could be the signal. Primers were designed to detect the common sequence of *aco2* (Aco2 common) and the long transcript of *aco2* (Aco2 NLS). The amount of each transcript was measured using RT-qPCR under high iron conditions: EMM+100 uM $FeCl_3$ or YE rich media (Normant et al., 2018) (Fig. IV-4). Unexpectedly, the amount of long transcripts did not increased in iron-rich conditions. In fact, the ratio of short and long transcript was nearly constant (about 2:1) regardless of the intracellular iron concentration. This result is also consistent with the northern blot result (Fig. I-7B) (Jung et al., 2015). Further research is required to find out the environmental signals or mechanisms of dual targeting of Aco2.

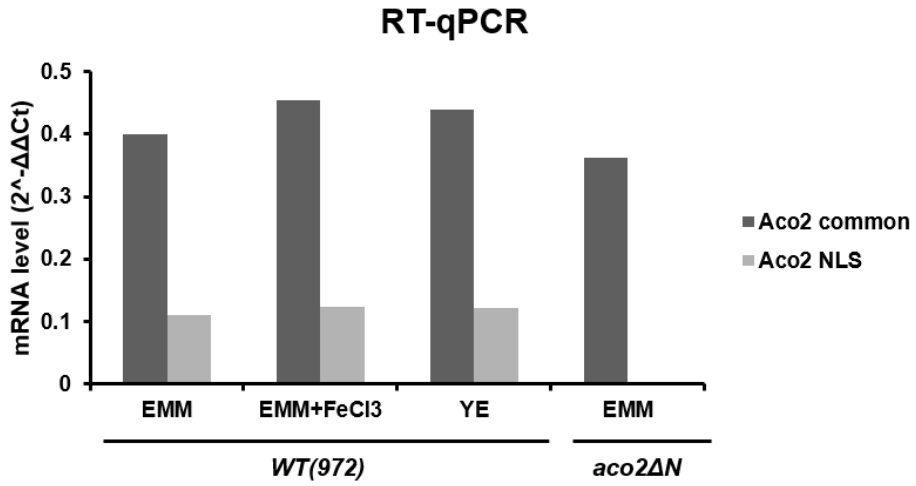

Figure IV-4. The amount of *aco2* transcripts under high iron conditions

Cells were incubated in EMM, EMM+ 100 uM FeCl3 or YE media at 30℃ for 3 h. The amount of the long transcript (Aco2 NLS) was about 0.3-fold than that of the toal *aco2* transcript.

REFERENCES

Alen, C., and Sonenshein, A.L. (1999). Bacillus subtilis aconitase is an RNA-binding protein. Proc Natl Acad Sci U S A *96*, 10412-10417.

Benjamin, J.A., and Masse, E. (2014). The iron-sensing aconitase B binds its own mRNA to prevent sRNA-induced mRNA cleavage. Nucleic Acids Res *42*, 10023-10036.

Boukouris, A.E., Zervopoulos, S.D., and Michelakis, E.D. (2016). Metabolic Enzymes Moonlighting in the Nucleus: Metabolic Regulation of Gene Transcription. Trends Biochem Sci *41*, 712-730.

Cam, H.P., and Whitehall, S. (2016). Analysis of Heterochromatin in Schizosaccharomyces pombe. Cold Spring Harb Protoc *2016*.

Carpy, A., Krug, K., Graf, S., Koch, A., Popic, S., Hauf, S., and Macek, B. (2014). Absolute proteome and phosphoproteome dynamics during the cell cycle of Schizosaccharomyces pombe (Fission Yeast). Mol Cell Proteomics *13*, 1925-1936.

Castello, A., Hentze, M.W., and Preiss, T. (2015). Metabolic Enzymes Enjoying New Partnerships as RNA-Binding Proteins. Trends Endocrinol Metab *26*, 746-757.

Chen, X.J., Wang, X., and Butow, R.A. (2007). Yeast aconitase binds and provides metabolically coupled protection to mitochondrial DNA. Proc Natl Acad Sci U S A *104*, 13738-13743.

Chen, X.J., Wang, X., Kaufman, B.A., and Butow, R.A. (2005). Aconitase couples metabolic regulation to mitochondrial DNA maintenance. Science *307*, 714-717.

Davis, R., and Shi, Y. (2014). The polyadenylation code: a unified model for the regulation of mRNA alternative polyadenylation. J Zhejiang Univ Sci B *15*, 429-437.

Encinar del Dedo, J., Gabrielli, N., Carmona, M., Ayte, J., and Hidalgo, E. (2015). A cascade of iron-containing proteins governs the genetic iron starvation response to promote iron uptake and inhibit iron storage in fission yeast. PLoS Genet *11*, e1005106.

Forsburg, S.L. (2001). The art and design of genetic screens: yeast. Nat Rev Genet *2*, 659-668.

Forsburg, S.L., and Rhind, N. (2006). Basic methods for fission yeast. Yeast *23*, 173-183.

Hardwick, S.W., Chan, V.S., Broadhurst, R.W., and Luisi, B.F. (2011). An RNA degradosome assembly in Caulobacter crescentus. Nucleic Acids Res *39*, 1449-1459.

Hayles, J., and Nurse, P. (2018). Introduction to Fission Yeast as a Model System. Cold Spring Harb Protoc *2018*.

Hayles, J., Wood, V., Jeffery, L., Hoe, K.L., Kim, D.U., Park, H.O., Salas-Pino, S., Heichinger, C., and Nurse, P. (2013). A genome-wide resource of cell cycle and cell shape genes of fission yeast. Open Biol *3*, 130053.

Herrick, D., Parker, R., and Jacobson, A. (1990). Identification and comparison of stable and unstable mRNAs in Saccharomyces cerevisiae. Mol Cell Biol *10*, 2269-2284.

Holoch, D., and Moazed, D. (2015). RNA-mediated epigenetic regulation of gene expression. Nat Rev Genet *16*, 71-84.

Jacques, J.F., Mercier, A., Brault, A., Mourer, T., and Labbe, S. (2014). Fra2 is a co-regulator of Fep1 inhibition in response to iron starvation. PLoS One *9*, e98959.

Jbel, M., Mercier, A., Pelletier, B., Beaudoin, J., and Labbe, S. (2009). Iron activates in vivo DNA binding of Schizosaccharomyces pombe transcription factor Fep1 through its amino-terminal region. Eukaryot Cell *8*, 649-664.

Jonstrup, A.T., Andersen, K.R., Van, L.B., and Brodersen, D.E. (2007). The 1.4-A crystal structure of the S. pombe Pop2p deadenylase subunit unveils the configuration of an active enzyme. Nucleic Acids Res *35*, 3153-3164.

Jung, S.-J. (2016). Multiple Functions of Aconitase-2 in Schizosaccharomyces pombe (Seoul National University).

Jung, S.J., Choi, Y., Lee, D., and Roe, J.H. (2019). Nuclear aconitase antagonizes heterochromatic silencing by interfering with Chp1 binding to DNA. Biochem Biophys Res Commun *516*, 806-811.

Jung, S.J., Seo, Y., Lee, K.C., Lee, D., and Roe, J.H. (2015). Essential function of Aco2, a fusion protein of aconitase and mitochondrial ribosomal protein bL21, in mitochondrial translation in fission yeast. FEBS Lett *589*, 822-828.

Kim, D.U., Hayles, J., Kim, D., Wood, V., Park, H.O., Won, M., Yoo, H.S., Duhig, T., Nam, M., Palmer, G., *et al.* (2010). Analysis of a genome-wide set of gene deletions in the fission yeast Schizosaccharomyces pombe. Nat Biotechnol *28*, 617-623.

Kim, J.K., Gabel, H.W., Kamath, R.S., Tewari, M., Pasquinelli, A., Rual, J.F., Kennedy, S., Dybbs, M., Bertin, N., Kaplan, J.M., *et al.* (2005). Functional genomic analysis of RNA interference in C. elegans. Science *308*, 1164-1167.

Kim, K.D., Kim, H.J., Lee, K.C., and Roe, J.H. (2011). Multi-domain CGFS-type glutaredoxin Grx4 regulates iron homeostasis via direct interaction with a repressor Fep1 in fission yeast. Biochem Biophys Res Commun *408*, 609-614.

Kuhl, I., Dujeancourt, L., Gaisne, M., Herbert, C.J., and Bonnefoy, N. (2011). A genome wide study in fission yeast reveals nine PPR proteins that regulate mitochondrial gene expression. Nucleic Acids Res *39*, 8029-8041.

Labbe, S., Khan, M.G., and Jacques, J.F. (2013). Iron uptake and regulation in Schizosaccharomyces pombe. Curr Opin Microbiol *16*, 669-676.

Liu, J., Li, Y., Chen, J., Wang, Y., Zou, M., Su, R., and Huang, Y. (2018). The fission yeast Schizosaccharomyces pombe Mtf2 is required for mitochondrial cox1 gene expression. Microbiology (Reading) *164*, 400-409.

Malecki, M., Bitton, D.A., Rodriguez-Lopez, M., Rallis, C., Calavia, N.G., Smith, G.C., and Bahler, J. (2016). Functional and regulatory profiling of energy metabolism in fission yeast. Genome Biol *17*, 240.

Malecki, M., Viegas, S.C., Carneiro, T., Golik, P., Dressaire, C., Ferreira, M.G., and Arraiano, C.M. (2013). The exoribonuclease Dis3L2 defines a novel eukaryotic RNA degradation pathway. EMBO J *32*, 1842-1854.

Mao, Y., and Chen, C. (2019). The Hap Complex in Yeasts: Structure, Assembly Mode, and Gene Regulation. Front Microbiol *10*, 1645.

Matsuyama, A., Arai, R., Yashiroda, Y., Shirai, A., Kamata, A., Sekido, S., Kobayashi, Y., Hashimoto, A., Hamamoto, M., Hiraoka, Y., *et al.* (2006). ORFeome cloning and global analysis of protein localization in the fission yeast Schizosaccharomyces pombe. Nat Biotechnol *24*, 841-847.

Mercier, A., Watt, S., Bahler, J., and Labbe, S. (2008). Key function for the CCAAT-binding factor Php4 to regulate gene expression in response to iron deficiency in fission yeast. Eukaryot Cell *7*, 493-508.

Mourer, T., Jacques, J.F., Brault, A., Bisaillon, M., and Labbe, S. (2015). Shu1 is a cell-surface protein involved in iron acquisition from heme in Schizosaccharomyces pombe. J Biol Chem *290*, 10176-10190.

Mukherjee, K., Gardin, J., Futcher, B., and Leatherwood, J. (2016). Relative contributions of the structural and catalytic roles of Rrp6 in exosomal degradation of individual mRNAs. RNA *22*, 1311-1319.

Normant, V., Mourer, T., and Labbe, S. (2018). The major facilitator transporter Str3 is required for low-affinity heme acquisition in Schizosaccharomyces pombe. J Biol Chem *293*, 6349-6362.

Parker, R., and Song, H. (2004). The enzymes and control of eukaryotic mRNA turnover. Nat Struct Mol Biol *11*, 121-127.

Pelletier, B., Beaudoin, J., Mukai, Y., and Labbe, S. (2002). Fep1, an iron sensor regulating iron transporter gene expression in Schizosaccharomyces pombe. J Biol Chem *277*, 22950-22958.

Pelletier, B., Beaudoin, J., Philpott, C.C., and Labbe, S. (2003). Fep1 represses expression of the fission yeast Schizosaccharomyces pombe siderophore-iron transport system. Nucleic Acids Res *31*, 4332-4344.

Pelletier, B., Trott, A., Morano, K.A., and Labbe, S. (2005). Functional characterization of the iron-regulatory transcription factor Fep1 from Schizosaccharomyces pombe. J Biol Chem *280*, 25146-25161.

Pouliot, B., Jbel, M., Mercier, A., and Labbe, S. (2010). abc3+ encodes an iron-regulated vacuolar ABC-type transporter in Schizosaccharomyces pombe. Eukaryot Cell *9*, 59-73.

Riemer, J., Hoepken, H.H., Czerwinska, H., Robinson, S.R., and Dringen, R. (2004). Colorimetric ferrozine-based assay for the quantitation of iron in cultured cells. Anal Biochem *331*, 370-375.

Satoh, R., Morita, T., Takada, H., Kita, A., Ishiwata, S., Doi, A., Hagihara, K., Taga, A., Matsumura, Y., Tohda, H., *et al.* (2009). Role of the RNA-binding protein Nrd1 and Pmk1 mitogen-activated protein kinase in the regulation of myosin mRNA stability in fission yeast. Mol Biol Cell *20*, 2473-2485.

Takeda, K., Starzynski, C., Mori, A., and Yanagida, M. (2015). The critical glucose concentration for respiration-independent proliferation of fission yeast, Schizosaccharomyces pombe. Mitochondrion *22*, 91-95.

Tandara, L., and Salamunic, I. (2012). Iron metabolism: current facts and future directions. Biochem Med (Zagreb) *22*, 311-328.

Telekawa, C., Boisvert, F.M., and Bachand, F. (2018). Proteomic profiling and functional characterization of post-translational modifications of the fission yeast RNA exosome. Nucleic Acids Res *46*, 11169-11183.

Touati, D. (2000). Iron and oxidative stress in bacteria. Arch Biochem Biophys *373*, 1-6.

Vlasova-St Louis, I., and Bohjanen, P.R. (2011). Coordinate regulation of mRNA decay networks by GU-rich elements and CELF1. Curr Opin Genet Dev *21*, 444-451.

Voss, J.E., Luisi, B.F., and Hardwick, S.W. (2014). Molecular recognition of RhlB and RNase D in the Caulobacter crescentus RNA degradosome. Nucleic Acids Res *42*, 13294-13305.

Wood, V., Gwilliam, R., Rajandream, M.A., Lyne, M., Lyne, R., Stewart, A., Sgouros, J., Peat, N., Hayles, J., Baker, S., *et al.* (2002). The genome sequence of Schizosaccharomyces pombe. Nature *415*, 871-880.

국문초록

생물체는 환경 변화를 감지함과 동시에 유전자 발현을 조절하는 효율적인 방식을 고안해왔다. 포유류의 aconitase 와 같이 다기능(moonlighting) 대사 효소를 통한 유전자 조절이 대표적인 예이다. 미토콘드리아 TCA 회로 효소로 잘 알려진 aconitase 는 세포 내 철이 부족할 경우 이를 인식하고 iron regulatory protein (IRP)로 작용하여 철 항상성과 관련된 mRNA 의 발현을 조절한다. Aconitase 의 다양한 기능은 박테리아부터 척추동물까지 여러 모델 생물체 내에서 보고된 바 있으나, 분열성 효모 *Schizosaccharomyces pombe* 내에서는 아직 많이 밝혀지지 않았다. 본 연구팀에서는 분열성 효모 내 aconitase 2 (Aco2)가 미토콘드리아 외에 핵 또는 세포질에도 존재함을 최초로 보고하였고, 미토콘드리아 내 Aco2 는 미토콘드리아 단백질의 번역, 핵 내 Aco2 는 heterochromatin 형성에 영향을 미친다는 사실을 밝혔다. 본 논문은 이에 대한 후속 연구로, 핵 내 존재하는 Aco2 의 또 다른 기능을 찾기 위해 Aco2 의 NLS (nuclear localization signal)를 제거한 균주(*aco2ΔNLS*)를 이용하여 전사체 분석(genome-wide transcriptome analysis)을 수행하였다. 야생형 균주와의 유전자 발현양을 비교분석한 결과, Aco2 NLS 결손 균주에서 유전자 발현이 크게 변화하는 유전자군으로 철 흡수 수송체 및 전자전달계 관련 유전자들이 발견되었다.

철은 세포 내 필수적인 원소이나 과다하게 존재할 경우 활성산소를 만들어 세포를 손상시킨다. 따라서 세포 내 철 항상성 유지는 매우 중요하고 철 흡수 유전자들의 발현은 Fep1 과 같은 전자억제인자에 의해 철저하게 조절된다. 그러나 Aco2 NLS 결손 균주에서는 철이 부족한 환경이 아님에도 불구하고 *Str1*, *Str3*, *Shu1* 과 같은 철 흡수 mRNA 의 발현이 증가해 있었다. mRNA decay assay 를 통해 Aco2 NLS 결손 균주에서는 철 흡수 mRNA 의 분해가 지연되어 세포 내 축적된 것이라는 것을 알 수 있었다. UV crosslinking RNA-IP (CLIP) 실험으로 Aco2 가 철 수송 mRNA 들과 직접 결합함을 관찰하였고, RNA 분해효소들 중 Rrp6 와 상호작용함을 co-IP 로 확인하였다. 따라서 핵 내 Aco2 는 철 흡수 mRNA 들이 RNA 분해효소에 의해 적절하게 분해되도록 도움으로써 세포 내 철 항상성 유지에 기여한다고 생각된다.

또한 Aco2 는 세포 호흡과 관련된 유전자들의 발현도 조절한다. 전사체 분석 결과 Aco2 NLS 결손 균주에서 미토콘드리아 내 ATP 합성과 관련된 전자전달계 유전자들의 발현이 크게 감소하는 것으로 나타났다. 전자전달계를 구성하는 단백질

유전자들은 대부분 핵 내 염색체에 코딩되어 있고 일부만 미토콘드리아 DNA 에 코딩되어 있다. Aco2 NLS 결손 균주에서는 특히 핵 내 코딩되어 있는 전자전달계 유전자들의 발현이 전체적으로 감소하였고, Qcr2, Cox13 같은 전자전달계 단백질의 양도 감소하였다. 세포 호흡이 요구되는 배지(non-fermentable carbon source media) 조건에서 Aco2 NLS 결손 균주의 생장이 크게 저해되는 것을 보아, 핵 내 Aco2 는 전자전달계 유전자들의 발현을 조절함으로써 세포 호흡까지 영향을 미치는 것으로 예상된다. mRNA decay assay 결과 전자전달계 mRNA 들의 분해속도는 야생형 균주에 비해 별 다른 차이가 없었으므로, Aco2 가 이 유전자들을 전사 과정에서 조절함을 짐작할 수 있다. 구체적인 조절 기작에 대해서는 추가 연구가 필요하다.

본 논문에서는 분열성 효모 내 Aco2 가 핵 또는 세포질에서 철 항상성 유지 및 세포 호흡과 관련된 유전자들의 발현 조절한다는 사실을 밝혔다. 특히 Aco2 에 의한 철 흡수 유전자들의 전사 후 조절 기작을 규명하여, 세포 내 철 항상성을 유지하는 새로운 방법을 제시하였다. 다기능 효소로서 진화적으로 보존된 기능과 분열성 효모 Aco2 가 갖는 위치적 특성을 고려해볼 때, Aco2 가 핵산 또는 단백질들과 상호작용하여 세포 내에서 또 다른 중요한 역할을 할 것으로 기대된다.

주요 단어: 분열성 효모, Aconitase, Iron-regulatory protein, 전사 후 조절, 다기능 대사 효소, RNA 분해, 전자 전달계, 세포 호흡